# A MODEL FOR SPONTANEOUS IMBIBITION AS A MECHANISM FOR OIL RECOVERY IN FRACTURED RESERVOIRS

P. Ø. ANDERSEN[A], S. EVJE[A,*] AND H. KLEPPE[A]

Abstract. The flow of oil and water in naturally fractured reservoirs (NFR) can be highly complex and a simplified model is presented to illustrate some main features of this flow system. NFRs typically consist of low-permeable matrix rock containing a high-permeable fracture network. The effect of this network is that the advective flow bypasses the main portions of the reservoir where the oil is contained. Instead capillary forces and gravity forces are important for recovering the oil from these sections. We consider a linear fracture which is symmetrically surrounded by porous matrix. Advective flow occurs only along the fracture, while capillary driven flow occurs only along the axis of the matrix normal to the fracture. For a given set of relative permeability and capillary pressure curves the behavior of the system is completely determined by the choice of two dimensionless parameters: (i) the ratio of time scales for advective flow in fracture to capillary flow in matrix $\alpha = \tau^f/\tau^m$; (ii) the ratio of pore volumes in matrix and fracture $\beta = V^m/V^f$. A characteristic property of the flow in the coupled fracture-matrix medium is the linear recovery curve (before water breakthrough) which has been referred to as the "filling fracture" regime [45], followed by a non-linear period, referred to as the "instantly filled" regime, where the rate is approximately linear with the square root of time. We derive an analytical solution for the limiting case where the time scale $\tau^m$ of the matrix imbibition becomes small relative to the time scale $\tau^f$ of the fracture flow (i.e., $\alpha \to \infty$), and verify by numerical experiments that the model will converge to this limit as $\alpha$ becomes large. The model provides insight into the role played by parameters like saturation functions, injection rate, volume of fractures vs. volume of matrix, different viscosity relations, and strength of capillary forces vs. injection rate. Especially, a scaling number $\omega$ is suggested that seems to incorporate variations in these parameters. An interesting observation is that at $\omega = 1$ there is little to gain in efficiency by reducing the injection rate. The model can be used as a tool for interpretation of laboratory experiments involving fracture-matrix flow as well as a tool for testing different transfer functions that have been suggested to use in reservoir simulators.

## 1. Introduction

Water flooding can be an efficient method for oil recovery in many reservoirs, as it provides pressure support and oil displacement. However, the efficiency depends on the ability of the water front to access all parts of the reservoir and displace the oil uniformly towards the producing wells. The injected water will typically be more mobile than the oil and concentrate into a "path of least resistance", where the pressure loss is minimal. In a uniform reservoir this path will be a straight line between injector and producer, while heterogeneities will move the path towards areas with higher permeability. In this paper our motivation is reservoirs that are naturally fractured: even on a local scale we can then distinguish such flow paths. The reservoir is divided into a dense network of connected highly permeable tunnels that only makes a small portion of the bulk, while the rest of the rock is low permeable, but is storage for much of the oil. As an example, consider the chalk reservoir Ekofisk in the North Sea: an unfractured section (i.e. a core sample) can have porosity around 30% and permeability of a few mD. However, from well tests the effective permeability (also considering fractures) is determined to be in the range of a 100 mD [23]. Because of this local heterogeneity the advective flow of water and oil will be concentrated to the fractures and oil contained in the matrix is not displaced efficiently by this mechanism. Capillary forces,

*Date*: October 28, 2013.

[A]University of Stavanger, NO-4068 Stavanger, Norway.

[*]Corresponding author.

Email address: steinar.evje@uis.no, pal.andersen@uis.no, hans.kleppe@uis.no.

This research of Evje has been supported by A/S Norske Shell.

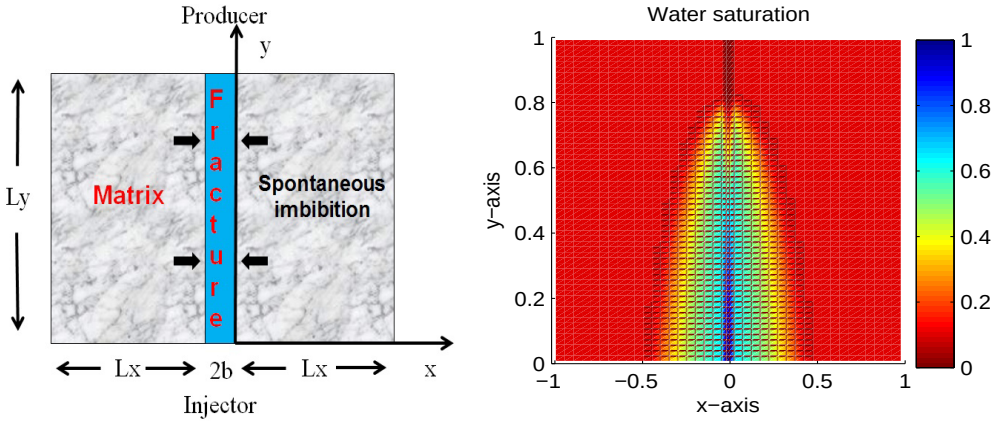


FIGURE 1. System geometry (left): reservoir is seen from above where a fracture of width $2b$ goes from injector to producer with length $L_y$. Matrix surrounds the fracture with total length $2L_x$. Spontaneous imbibition drives oil into the fracture, while water injection drives the mixture towards the producer along the fracture (right).

depressurization or gravity may play a greater role in mobilizing the oil where advective transport is low. Flooding the reservoir will efficiently displace oil in the channels and they become highly water-saturated. Capillary forces will draw water into the less permeable medium and return oil to the fractures, thus, lead to a redistribution of oil and water. This mechanism is referred to as spontaneous imbibition (SI). See Fig. 1 for an illustration of the fracture-matrix geometry and displacement of water along fracture due to viscous forces in combination with countercurrent imbibition in matrix due to capillary forces.

In works such as [19, 22, 24, 25] experimental observations from lab scale flooding through blocks or cores of porous material with and without layers of thin permeable fractures were presented. Using MRI techniques the authors obtained 3D images of phases and pores. Especially they illustrated how wettability and capillary forces are important for the distribution of phases in a fracture-matrix system. In [20] the authors considered a combined water-oil fracture-matrix model with special focus on the problem of formulating an appropriate boundary condition at the fracture-matrix interface.

The importance of fracture-matrix flow where imbibition is the driving mechanism for flow in matrix, has motivated for many works dealing with spontaneous imbibition. Analytical solutions of models describing spontaneous imbibition represent one aspect of this. For some recent works which contain a complete overview of various results in that direction, we refer to [54, 55]. By means of an analytical solution of the nonlinear diffusion equation representing SI [38], a general scaling group was proposed, which contains previously proposed groups as special cases, and used that to demonstrate a nice fit with many imbibition lab experiments for a wide range of viscosity ratios, different materials, different initial water saturations, and different length scales.

Research dealing with models for fracture-matrix flow seems essentially to be along two main lines: One approach is based on using an explicit discretization of both fracture and matrix, a so-called discrete fracture/discrete matrix (DFDM) approach [14, 27, 29, 48, 37, 53, 57]. Another commonly used approach is based on the dual-porosity idea where the geometry of fracture and matrix are represented by averaged properties [60]. The communication between fracture and matrix is taken care of through a transfer term. We refer to [12] for a nice overview and demonstration of this approach. In this setting, typically, the impact from matrix is taken into account in the fracture flow model by including a source/sink term of the following linear form [31, 12, 60]

$$T = \phi^m \beta_r (s^m_{eq} - s^m), \tag{1}$$

where $\beta_r$ is a rate constant, $\phi^m$ is the porosity, $s^m$ is the average saturation, and $s^m_{eq}$ is the maximal saturation in the matrix. However, this form seems more appropriate when it can be assumed that the fracture is instantly filled with water and takes a constant saturation. Various modifications have been introduced to account for different flow regimes and more general rate terms [12]. In [21] the authors develop a multi-rate mass transfer model for two-phase flow. The fracture model contains a non-local (in time) source/sink term that accounts for the interaction with the matrix region. Their approach allows to simulate a wide range of transfer rates.

We construct a combined fracture-matrix 1D+1D model in order to investigate the role of spontaneous imbibition as a recovery mechanism in an idealized geometry for different fracture-matrix flow regimes. More precisely, we consider flow along a single fracture from injector to producer well with porous matrix along the fracture being drained for oil, as illustrated in Fig. 1 (left). The system is solved numerically by an operator splitting approach. The description is similar to the dual-porosity formulation in that the fracture is considered as 1-dimensional with a source term relating to the transfer with matrix and that advection is neglected in matrix. Unlike the dual-porosity formulation, we solve the transport equation for the matrix locally and do not assume instantly filled fractures. In that sense our approach bears similarities to works like [14, 21]. A similar geometry was also studied in [58]. The authors discretized the fracture and implemented matrix imbibition using source terms with memory functions. They obtained a simplified 1D model for the 2D system which could account for the diffusive nature of capillary flow and non-equilibrium effects by using an appropriate memory function.

The proposed model allows a qualitative discussion of some questions of practical importance: (i) How does the fracture network affect the oil recovery? (ii) What is the role of the wetting state of the matrix? (iii) What is the role of capillary forces versus injection rate? (iv) What is the role played by volume of fractures compared to volume of matrix? (v) What is the role of different fluid properties like, e.g., viscosity? To answer some of these questions we derive relevant dimensionless parameters and investigate the related sensitivity on oil recovery and phase distribution. In particular, the model allows for a systematic study of the two flow regimes, the so-called "filling fracture" and the "instantly filled" regime reported and discussed in works like [45, 46]. A scaling number is suggested for characterizing flow in the considered fracture-matrix system. Numerical simulations are used to support this assumption. Also, analytical solutions are presented for the situation when the time scale of imbibition becomes small compared to the time scale of fracture flow. We demonstrate through numerical experiments that the 1D+1D model converges towards this analytical solution. The analytical solution describes the fracture-matrix flow when the "fracture filling" regime is dominating. This represents so-to-say the opposite situation of what has been studied in works like [12, 31] where analytical solutions have been derived when fracture is instantly filled with water and takes a constant saturation. A possible application of the model is to use it for interpretation of lab experiments in simpler fracture-matrix geometries [45, 46, 24, 19] as well as to test possibilities and limitations of various transfer rate functions of the form (1).

The rest of the paper is organized as follows: In Section 2 the reduced 1D+1D model is derived from basic laws well known in petroleum literature. The model is scaled with respect to some representative parameters to derive dimensionless numbers characterizing the system. In Section 3 we apply the model by varying key parameters, one at a time, to demonstrate their effect on the distribution of phases and resulting oil recovery. We also demonstrate the validity of the assumptions made by comparing the 1D+1D model with a discretization of the full 2D model. The sensitivity study is summarized in a scaling number that characterizes the flow behavior. We also verify the numerical solution of the model by comparing it with analytical solutions.

## 2. System description and modeling

2.1. **Transport equations.** The transport equations for incompressible, immiscible oil-water flow in porous rock reads

$$\begin{aligned} \partial_t(\phi s_o) &= -\nabla \cdot (\phi \mathbf{v}_o), \\ \partial_t(\phi s_w) &= -\nabla \cdot (\phi \mathbf{v}_w), \end{aligned} \tag{2}$$

where $\phi$ is porosity, $s_i$ saturation ($i = w, o$) and it has been assumed that there are no external source terms. The phase velocities are given by Darcy's law:

$$\phi \mathbf{v}_i = -\mathbf{K}\lambda_i[\nabla p_i - \rho_i g \nabla z], \qquad \lambda_i = \frac{k_{ri}}{\mu_i} \qquad (i = w, o), \tag{3}$$

where $\mathbf{v}_i$ is pore velocity, $p_i$ pressure, $\rho_i$ density, $\lambda_i$ mobility, $k_{ri}$ relative permeability and $\mu_i$ viscosity of oil ($i = o$) or water ($i = w$). $\mathbf{K}$ is absolute permeability tensor, z is positive direction upwards (opposite the direction of gravity) and $g$ the gravity acceleration constant. The saturations and pressures are constrained by the following conditions:

$$s_w + s_o = 1, \qquad p_o - p_w = p_c(s_w), \tag{4}$$

where $p_c$ is capillary pressure, which is a known function. Summing the equations for oil and water,

$$\partial_t(\phi(s_o + s_w)) = -\nabla \cdot (\phi(\mathbf{v}_o + \mathbf{v}_w)) = -\nabla \cdot (\phi \mathbf{v}_T) = 0, \tag{5}$$

shows that the total Darcy velocity $\phi \mathbf{v}_T = \phi(\mathbf{v}_o + \mathbf{v}_w)$ has zero divergence, i.e. there is no source/sink. We introduce the so called fractional flow function defined as

$$f_w = \frac{\lambda_w}{\lambda_w + \lambda_o} = \Big(1 + \frac{\mu_w}{\mu_o}\frac{k_{ro}}{k_{rw}}\Big)^{-1}. \tag{6}$$

Also define $\Delta\rho \equiv \rho_w - \rho_o$. Using equations (4)-(6) we remove the variables $p_w, p_o, s_o$ and replace them by $p_c(s_w), \mathbf{v}_T, f_w(s_w)$. The system (2) can then be written into (7) where the change in storage is affected by an advective/gravitational term and a capillary diffusion term.

$$\partial_t(\phi s_w) + \nabla \cdot \Big(\phi \mathbf{v}_T f_w(s_w) + \mathbf{K} g[\lambda_o f_w](s_w)\Delta\rho\nabla z\Big) = -\nabla \cdot \Big(\mathbf{K}[\lambda_o f_w](s_w)\nabla p_c(s_w)\Big). \tag{7}$$

The velocity field $\mathbf{v}_T$ and $s_w$ (denoted $s$ in the following) are the variables that must be calculated.

2.2. **Geometry of fracture-matrix system.** In this paper we consider a system in the x-y-plane consisting of a single fracture, surrounded by matrix on both sides in a symmetrical rectangular geometry, as illustrated in Fig. 1. The fracture is located along the y-axis, has length $L_y$ and width $2b$, while the depth into matrix is $L_x$. For simplicity flow in z-direction (including gravity) is discarded. The fracture and matrix domains are given by

$$\begin{aligned} \Omega^f &= \{(x, y) : -2b < x < 0; \quad 0 < y < L_y\}, \\ \Omega^m &= \{(x, y) : -2b - L_x < x < -2b, \quad 0 < x < L_x; \quad 0 < y < L_y\}. \end{aligned} \tag{8}$$

The two domains have different properties in terms of permeability, porosity and flow functions. The outer boundaries of $\Omega^m$ are closed and the boundary condition for the model is then described by the no-flow boundary condition: $\mathbf{v}_i \cdot \mathbf{n} = 0$, where $i = w, o$, and $\mathbf{n}$ is the outer normal to the boundary of $\Omega^m$. The fracture has an injector side and a producer side

$$\Gamma^{inj} = \{(x, y) : -2b < x < 0; \quad y = 0\}, \qquad \Gamma^{prod} = \{(x, y) : -2b < x < 0; \quad y = L_x\} \tag{9}$$

where appropriate boundary conditions are assigned.

2.3. **A simplified fracture-matrix model.** We seek a simplified model that can represent important aspects of the full 2D model (4)–(7) combined with the fracture-matrix domain, as described by (8). The model we consider represents a simplification of real reservoirs in different aspects:

- A single fracture drains oil from surrounding matrix.
- Rock properties (porosity, permeability) are homogeneous within matrix and fracture.
- Advective motion in the matrix is ignored and matrix oil is recovered by spontaneous imbibition only.
- Average properties of the fracture are sufficient to describe the state near the fracture-matrix interface and can be used for modeling fluid transfer.
- Capillary motion occurs only perpendicular to the fracture.
- Relative permeability and capillary pressure curves are given respectively for the fracture and matrix region. Continuity in the capillary pressure at the fracture-matrix interface is assumed.

We note that real NFRs are described by complex networks of fractures intertangled between matrix blocks of highly varying dimensions and connectivity, as illustrated in [21]: a multi-rate dual porosity model was used to capture the different time scales of recovery resulting from the block size distribution. Aside from spontaneous imbibition, the matrix oil can be recovered by gravity drainage, advective displacement, depressurization and others, see a brief discussion in [17]. Excluding advection in matrix is a common assumption in NFR modeling (i.e. dual porosity) as the fracture network usually is much more permeable than the matrix. Depending on permeability contrast, fracture density and orientation this is not always a good assumption. Neglecting capillary flow parallel with the fracture direction is based on a scaling argument, see Section 2.4, and is reasonable if the water moves much faster inside the fracture by advection than inside the matrix by capillary motion. The flow of oil and water at the matrix-fracture interface is characterized by droplets forming and detaching [20, 19]. Also, if the fracture width is low a liquid bridge can form across and support capillary continuity from one matrix block to another, see [16] for a discussion.

2.3.1. *Matrix region.* Consider the matrix domain, $\Omega^m$. Advective transport effects are ignored, i.e., terms associated with the total velocity $\mathbf{v}_T^m = 0$ are neglected. The model (7) is then reduced to the following diffusion equation:

$$\partial_t(\phi^m s) = -\partial_x\Big(K^m[\lambda_o^m f_w^m](s)\partial_x p_c^m(s)\Big) - \partial_y\Big(K^m[\lambda_o^m f_w^m](s)\partial_y p_c^m(s)\Big). \tag{10}$$

2.3.2. *Fracture region.* Next, consider the fracture domain, $\Omega^f$. It is assumed that advection occurs only in y-direction. From (7) we then obtain the following equation:

$$\partial_t(\phi^f s) = -\partial_y\Big(\phi^f v_T^f f_w^f(s)\Big) - \partial_y\Big(K^f[\lambda_o^f f_w^f](s)\partial_y p_c^f(s)\Big) - \partial_x\Big(K^f[\lambda_o^f f_w^f](s)\partial_x p_c^f(s)\Big). \tag{11}$$

We now consider the fracture as a 1-dimensional line of constant width $2b$. The mass transfer with the matrix is accounted for using a source term $q_w$ that is positive when water enters the fracture. The model takes the form

$$\partial_t(2b\phi^f s) = -\partial_y\Big(2b\phi^f v_T^f f_w^f(s)\Big) - \partial_y\Big(2bK^f[\lambda_o^f f_w^f](s)\partial_y p_c^f(s)\Big) + q_w. \tag{12}$$

In (12) we implicitly assume that the flow within the fracture is sufficiently strong to ensure a perfect mixing across the fracture width $2b$. The source term is defined such that the flux entering the fracture corresponds to the diffusive flux leaving the matrix region from both sides, symmetrically. That is,

$$q_w = 2(-\phi v_w)|_{x=0} = 2\Big(-K[\lambda_o f_w](s)\partial_x p_c(s)\Big)|_{x=0}. \tag{13}$$

Note that the transfer term is based purely on capillary motion due to a gradient in capillary pressure between matrix and fracture. The term is evaluated at the interface and must account for properties of both regions. Combining (12) and (13) we get the following 1D version of (11)

$$\partial_t(\phi^f s) = -\partial_y\Big(\phi^f v_T^f f_w^f(s)\Big) - \partial_y\Big(K^f[\lambda_o^f f_w^f](s)\partial_y p_c^f(s)\Big) - \frac{1}{b}\Big(K[\lambda_o f_w](s)\partial_x p_c(s)\Big)|_{x=0}. \tag{14}$$

**Remark 1.** *The model we formulate represents a combination of ideas employed in works like* [35, 20, 59, 30, 43]*. The model boils down to a Buckley-Leverett model for the fracture flow equipped with a transfer term accounting for mass transfer with the adjacent matrix. The water-oil transport mechanism of the matrix region is described by the nonlinear diffusion equation representing spontaneous imbibition similar to the one employed in* [43, 30, 20]*. At the current stage we do not include modelling of finer mechanisms on the fracture-matrix interface in terms of any droplet detachment model as discussed in* [20] *for a laboratory scale model. It is assumed that the coupling between fracture and matrix can be accounted for through the continuity in capillary pressure at the interface between fracture and matrix.*

2.4. **Scaling and a reduced 1D+1D model.** We now scale the transport system by introducing the following dimensionless variables:

$$x' = \frac{x}{L_x}, \qquad x'_f = x' \frac{\phi^f}{\phi^m}, \qquad y' = \frac{y}{L_y}, \qquad t' = \frac{t}{\tau^f}, \tag{15}$$

where the choice of $\tau^f$ corresponds to the time of injecting 1 fracture volume of water (see below). The dimensionless parameters and functions we use are

$$\mu' = \frac{\mu}{\mu_o}, \qquad p'_c(s) = \frac{p_c(s)}{P_{c,max}} = J(s), \qquad b' = \frac{b\phi^f}{L_x\phi^m}, \qquad \lambda'_i(s) = \lambda_i(s)\mu_o. \tag{16}$$

We introduce the following reference times:

(i) Advective flow in the fracture, $\tau^f = \frac{L_y}{v_T^f}$ (s);

(ii) Capillary flow in the matrix, $\tau^{c,m} = \frac{\phi^m L_x^2 \mu_o}{K^m P_{c,max} D_{av}^m}$ (s);

(iii) Capillary flow in the fracture, $\tau^{c,f} = \frac{\phi^f L_y^2 \mu_o}{K^f P_{c,max} D_{av}^f}$ (s).

Note that $D_{av}$ is a dimensionless average of the scaled capillary diffusion coefficient $\lambda_o f_w J'(s)$ taken over the saturation range where water will flow:

$$D_{av} = \frac{1}{s_{eq} - s_0} \int_{s_0}^{s_{eq}} \lambda_o(s) f_w(s) \frac{dJ(s)}{ds} ds, \tag{17}$$

$s_{eq}$ corresponds to the endpoint for imbibition, $s_0$ is initial saturation. $D_{av}$ is used to account for the shape and magnitude of the scaled flow curves by scaling with their average. Note that by this measure $D_{av}^{-1}\lambda_o f_w J'(s) \sim O(1)$ for a representative range of saturations.

After scaling, the coupled system (10) and (14) can be expressed in the following form (skipping prime notation):

$$\begin{aligned} \partial_t s =& -\alpha \partial_x([D_{av}^m]^{-1}\lambda_o^m f_w^m \partial_x J^m) - \alpha \frac{L_x^2}{L_y^2} \partial_y \Big( [D_{av}^m]^{-1} \lambda_o^m f_w^m \partial_y J^m \Big) \\ & (0 < x < 1; \quad 0 < y < 1) \end{aligned} \tag{18}$$

$$\begin{aligned} \partial_t s =& -\partial_y f_w^f - \gamma \partial_y \Big( [D_{av}^f]^{-1} [\lambda_o^f f_w^f](s) \partial_y J^f(s) \Big) - \alpha\beta \Big( [D_{av}^m]^{-1} \lambda_o^m f_w^m \partial_x J^m \Big)|_{x=0^+} \\ & (-2/\beta < x < 0; \quad 0 < y < 1), \end{aligned} \tag{19}$$

where we have introduced the following dimensionless numbers:

$$\alpha = \frac{\tau^f}{\tau^{c,m}} = \frac{L_y}{v_T^f} \frac{K^m P_{c,max} D_{av}^m}{\phi^m L_x^2 \mu_o}, \qquad \beta = \frac{1}{b'} = \frac{L_x \phi^m}{b\phi^f}, \qquad \gamma = \frac{\tau^f}{\tau^{c,f}} = \frac{K^f D_{av}^f P_{c,max}}{\mu_o v_T^f L_y \phi^f}. \tag{20}$$

It will be assumed that $\alpha L_x^2/L_y^2 << 1$ such that matrix capillary flow in y-direction is negligible (2nd term on RHS of (18) is removed). This is relevant if the water travels faster by advection in the fracture than by imbibition in the matrix in y-direction.

Also, we assume $\gamma << 1$ such that any capillary gradient in the fracture is negligible (this removes the 2nd term on RHS of (19)). Note that the velocity in the fracture $v_T^f \propto K^f$ and the capillary pressure as included in $D_{av}^f P_{c,max}$ varies with permeability according to Leverett's scaling: $P_c = \sigma \cos(\theta)(\sqrt{K/\phi})^{-1}\tilde{J}$, where $\sigma$ is oil-water interfacial tension, $\theta$ contact angle and $\tilde{J}$

a scaled capillary pressure function. It then follows that $\gamma \propto \frac{1}{L_y\sqrt{K^f}}$ and will become negligible for large $K^f$ or $L_y$, as will be assumed. The resulting system of equations can then be described as:

$$\partial_t s = -\alpha\partial_x([D^m_{av}]^{-1}\lambda^m_o f^m_w \partial_x J^m), \qquad (0 < x < 1; \quad 0 < y < 1), \tag{21}$$

$$\partial_t s = -\partial_y f^f_w - \alpha\beta\Big([D^m_{av}]^{-1}\lambda^m_o f^m_w \partial_x J^m\Big)|_{x=0^+}, \qquad (-2/\beta < x < 0; \quad 0 < y < 1). \tag{22}$$

**Remark 2.** *The time scale for imbibition $\tau^{c,m}$ is most reasonable when the capillary diffusion coefficient behaves close to its average value. In different works this average value has been used instead of the full coefficient to simplify the matrix modelling: In* [45] *this assumption was used to derive analytical solutions for combined fracture-matrix flow. We solve using the nonlinear coefficient, but are interested in the average value to account for the effect on the time scale. Analytical solution for co- and countercurrent imbibition have been developed* [38]*. In* [55, 56] *the authors considered these analytical solutions to scale a variety of lab imbibition experiments. However, these solutions were constructed for constant saturation boundaries and may not account for the changing boundary conditions at the interface observed during matrix-fracture flow.*

**Remark 3.** *The relevance of the reduced 1D+1D model composed of* (21) *and* (22) *will be evaluated in Section 3 by comparing with a discretization of the full 2D model. Then the simplified model will be used to carry out a study of the role played by different parameters like $\alpha$ and $\beta$. We also demonstrate how to obtain an analytical solution of the model* (21) *and* (22) *for the limiting case when $\alpha \to \infty$ (i.e., capillary forces in matrix become dominating) and use this analytical solution to check the validity of the numerical solution of the 1D+1D model.*

2.5. **Relative permeability and capillary pressure functions.** Introduce the normalized water saturation $s^* = \frac{s-s_{wr}}{1-s_{or}-s_{wr}}$, where $s_{wr}$ and $s_{or}$ are residual saturation values at which the phase does not flow during advective displacement. The relative permeabilities are modeled using Corey type correlations [9] given as

$$k_{rw}(s) = k^*_w(s^*)^{N_w}, \qquad k_{ro}(s) = k^*_o(1-s^*)^{N_o}, \qquad s_{wr} \le s \le 1 - s_{or}. \tag{23}$$

$N_w$ and $N_o$ are the Corey exponents and $k^*_w$ and $k^*_o$ are end point values. In the fracture the relative permeabilities are assumed to be linear:

$$k_{rw} = s, \qquad k_{ro} = (1-s). \tag{24}$$

The oil-water capillary pressure curves are defined through a dimensionless function $J$ of the form $p_c(s) = P_{c,max}J(s^*)$. As a model for mixed-wet media (see Remark 4) we let the imbibition curves $J^m(s)$ for the matrix be given by the following correlation:

$$J^m(s) = \frac{a_1}{1+k_1 s^*} - \frac{a_2}{1+k_2(1-s^*)} + b. \tag{25}$$

Curves are specified by the parameters $a_i, b, k_i$. A brief discussion of this correlation and numerical parameters are given in Appendix A, see also Remark 5. In accordance with other works [59, 24, 16] we assume the capillary pressure in the fracture is zero:

$$J^f(s) = 0. \tag{26}$$

Zero fracture capillary pressure has been widely employed in the numerical simulation of fractured reservoirs, however, this remains to be a controversial topic. Different works have been carried out that involves formulation of the formation, growth, and detachment of liquid bridges causing capillary continuity between matrix blocks [22, 24, 16, 19]. This may imply that other choices for fracture capillary pressure are more realistic. In [44, 24] historymatching experiments indicated more advanced curves.

**Remark 4.** *Mixed wettability means that a rock has a heterogeneous distribution of oil-wet and water-wet sites at the porescale* [50]*. A mixed-wet rock has positive values of capillary pressure at low saturations and negative values at high saturations* [8, 56]*. The saturation where the capillary pressure vanishes corresponds to where the rock cannot draw in more water by capillary forces. Rock wettability is important since higher affinity for water is characterized by imbibition to higher water*

*saturations. Relative permeability and capillary pressure are both affected by wettability* [6, 7]*. Pore scale models can produce saturation curves by specifying pore space geometry and wetting conditions at the surfaces, see* [65, 13, 61, 8]*. Using 3D pore network models it was shown* [8] *that mixed-wet media with a high fraction of oil-wet sites could have relative permeabilities two orders of magnitude lower than strongly water-wet media. The authors showed that the different time scales of imbibition observed in the experimental work* [64] *could be attributed greatly to this variation in relative permeability for the different wettability states.*

**Remark 5.** *The selected capillary pressure correlation* (25) *is not a limitation of the model. The correlation is appropriate for mixed-wet data and does not require any regularization (in the sense that the function and its derivative are bounded). Known correlations from the literature can also be applied such as Brooks-Corey* [9] *and van Genuchten* [62] *for water-wet media or Skjaeveland* [51] *and Masalmeh* [36] *for mixed-wet media, but they require some type of regularization since they diverge near the residual saturations. This is easily implemented by modifying the Pc-curves to have a fixed gradient near the residual saturations such that both the function and its derivative are continuous. See also* [34] *for an example of a bounded correlation.*

2.6. **Initial, boundary and interface conditions.** In addition to the transport equations the system is equipped with initial conditions of the following form:

$$s(x, y, t = 0) = s_0(x, y). \tag{27}$$

Boundary conditions for the fracture at the injector is given by the composition of the injected fluid:

$$s(\Gamma^{inj}, t) = s_{inj}. \tag{28}$$

The boundary at the producer is treated as a point on a semi-infinite axis, i. e. we can write

$$s(-2/\beta < x < 0, \infty, t) = s_\infty. \tag{29}$$

The boundary at the exterior of the matrix can be assumed to be closed or symmetric. In either case there is no flow

$$(\lambda_o^m f_w^m \partial_x J^m)|_{x=1} = 0. \tag{30}$$

At the interface between fracture and matrix we assume continuity in capillary pressure, i.e.,

$$J^m|_{x=0} = J^f|_{x=0}. \tag{31}$$

## 3. Numerical investigations

The numerical solution procedure that is employed to solve the scaled system is described in Appendix B. In this section we explore the behavior of the model by considering its sensitivity to different input parameters.

3.1. **Model input.** Necessary constant input parameters are given in Table 1. We also require curves for capillary pressure given by $J(s)$ and relative permeability $k_{ri}(s)$ for both the fracture and the porous matrix, see plots in Fig. 2. Parameters used as input for the matrix functions are given in Table 2 in Appendix A. The saturation curves of the matrix have been considered for two cases that we term preferentially water-wet (POW) or preferentially oil-wet (PWW), note Remark 6. This is represented by 2 different sets of curves: $(k_{ro}^{m,pow}, k_{rw}^{m,pow}, J^{m,pow})$ and $(k_{ro}^{m,pww}, k_{rw}^{m,pww}, J^{m,pww})$. The PWW curve set, accompanied by the parameters in Table 1, will be our reference case. Based on this we calculate the following parameters:

$$D_{av,0} = 0.0120, \qquad \tau_0^f = 10d, \qquad \tau_0^m = 804d, \qquad \alpha_0 = 0.0124, \qquad \beta_0 = 20, \qquad \frac{\mu_w}{\mu_o} = 1. \tag{32}$$

The index '0' corresponds to these base input data. $\alpha$ and $\beta$ are given by (20). Interpretation of these values will be explained in later sections.

The fracture saturation curves are given by (24) and (26). With $\mu_o = \mu_w$ and linear relative permeabilities it follows by definition (6) that the flow function of the fracture is a straight line.

| | | | |
|---|---|---|---|
| Well spacing, $L_y$ | 100m | Fracture pore velocity, $v_T^f$ | 10m/d |
| Fracture aperture, $2b$ | 0.001m | Matrix permeability, $K^m$ | 5mD |
| Fracture porosity, $\phi^f$ | 1.0 | Oil viscosity, $\mu_o$ | 1cP |
| Matrix porosity, $\phi^m$ | 0.20 | Water viscosity, $\mu_w$ | 1cP |
| Fracture spacing, $2L_x$ | 0.10m | Initial capillary pressure, $P_{c,max}$ | 120Pa |

TABLE 1. Constant parameters used for reference case simulations. In addition, a set of relative permeability and capillary pressure curves must be specified for matrix and fracture.

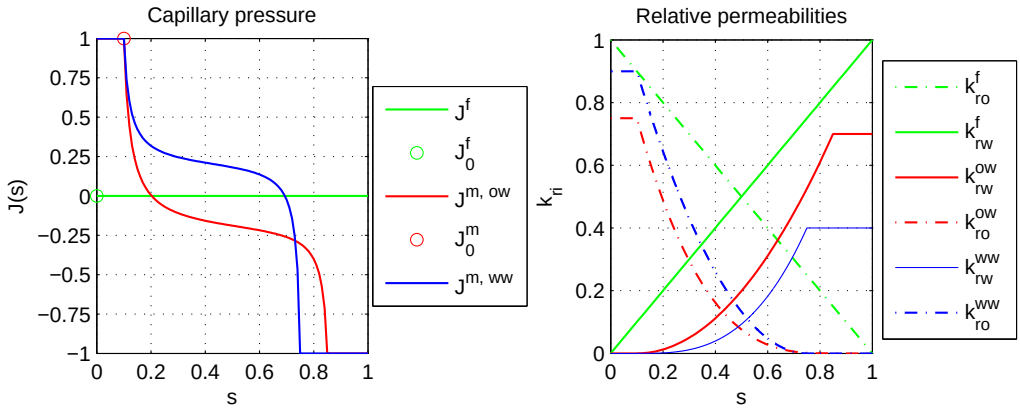


FIGURE 2. Input curves for capillary pressure (left) and relative permeability (right). Green curves represent fracture. Two curve sets are considered for the matrix: preferentially oil-wet (red) and preferentially water-wet (blue). $J_0^f$ and $J_0^m$ denote initial states.

The matrix has been assigned an initial saturation $s_0^m = 0.10$ at which the capillary pressure takes its highest value, i.e. $J^m(s_0^m) = 1$. As the fracture has zero capillary pressure, $J^f = 0$, we set $s_0^f = 0.0$, since any initial water would spontaneously imbibe into the matrix.

For the numerical examples that follow the model was discretized using $N_x = 40$ cells along the matrix and $N_y = 120$ cells along the fracture. The splitting step was set to 1/100 of the time it takes to inject 1 fracture volume. This ensures that the advancing water in fracture interacts frequently with the matrix. See also Section 3.2.9 where we study the effect of these numerical parameters.

**Remark 6.** *The matrix saturation curves used in the examples (see Fig. 2) are qualitative in nature and may not give an exact representation of wettability since they are not based on experimental measurements or derived from pore scale simulations. The capillary pressure curves for the preferentially water-wet set was defined by the ability to imbibe more water than the set termed preferentially oil-wet. Also, it was assumed that the relative permeability of a phase would be lower in the set where it was more wetting. This was reported for fractionally wetted media* [7] *since the wetting phase would tend to flow through more of the narrow, low-permeable pores.*

## 3.2. **Investigations of basic features of the 1D+1D model.**

3.2.1. *Role of saturation curves.* We will compare the base case (having PWW curves) to a case where the flow curves are given by the POW state as depicted in Fig. 2. As seen from the capillary pressure curves in Fig. 2, the PWW matrix can spontaneously imbibe water until $s = 0.7$ while imbibition in the POW matrix stops when $s = 0.2$. The characteristics of each set $(k_{rw}, k_{ro}, J)$ can be summarized by the capillary diffusion coefficient $D_{av}^m$ and the imbibition potential $\Delta s = s_{eq} - s_0$:

$$D_{av}^{m,pww} = 0.0120 \qquad \Delta s^{m,pww} = 0.6, \qquad D_{av}^{m,pow} = 0.0152, \qquad \Delta s^{m,pow} = 0.1. \tag{33}$$

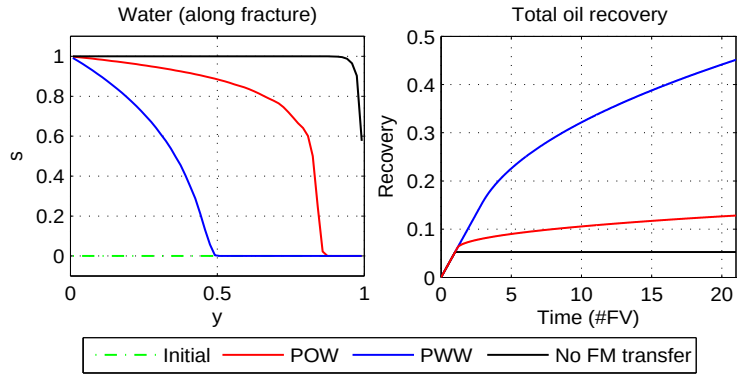


FIGURE 3. Role of saturation curves. Left: Water saturation profile in fracture (after having injected 1 FV) is more retained by imbibition for PWW matrix than POW matrix. Right: Recovery profile depends strongly on the imbibition potential $\Delta s$ which is greater for the PWW matrix.

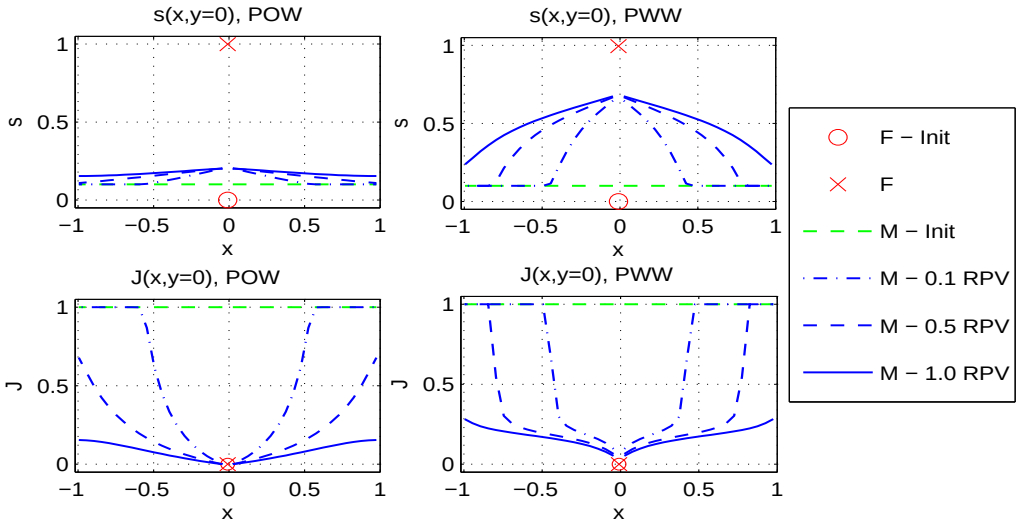


FIGURE 4. Water saturation (top) and capillary pressure (bottom) along matrix at $y = 0$ for POW (left) and PWW (right) matrix. Matrix profiles at $y = 0$ of capillary pressure $J$ and water saturation after injecting 0.1, 0.5 and 1.0 RPV of water (middle). POW matrix imbibes less water than PWW matrix.

$D_{av}$ is similar in both cases, but more water can imbibe in the PWW case.

Injection of 1 fracture volume (FV) of water is illustrated in Fig. 3 (left). If there is no imbibition the water front (represented by water saturation in the fracture) will have reached the producer position. When water imbibes, the water front along the fracture is delayed. Since more water is retained in the PWW matrix we observe a greater delay of the water front for this case.

The behavior along the matrix (x-axis) at $y = 0$ is shown in Fig. 4: Due to the high capillary pressure in the matrix water will imbibe and expel oil back to the fracture. The increasing matrix water saturation reduces the matrix capillary pressure and imbibition proceeds until it equals that of the fracture. Because of the decreasing capillary pressure the force drawing water into the fracture is reduced making the imbibition rate decrease. At a given point the rate of imbibition depends also on the supply of water and removal of expelled oil as dictated by the transport in the fracture. Especially, imbibition cannot begin somewhere before the water front has arrived.

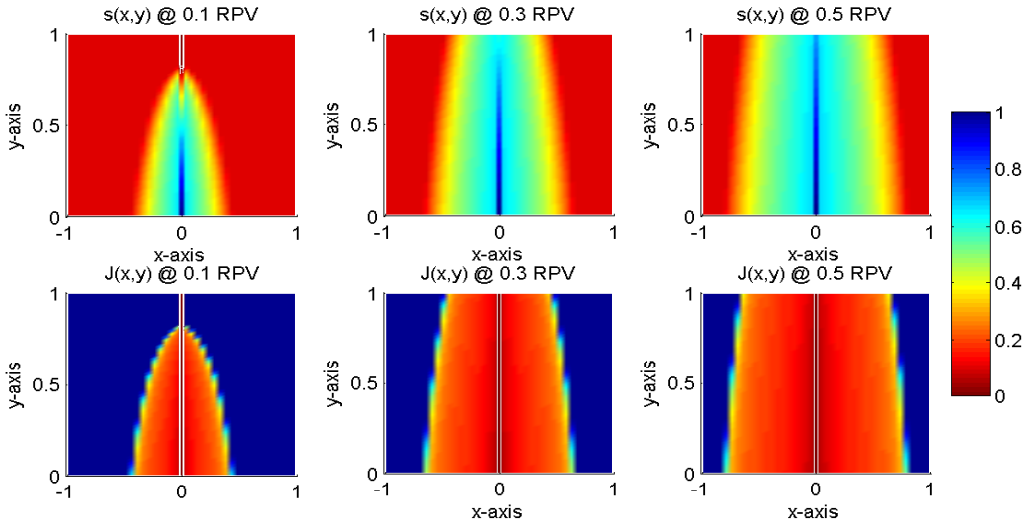


FIGURE 5. Distributions of water saturation $s$ (up) and capillary pressure $J$ (below) for base case after flooding 0.1 (left), 0.3 (middle) and 0.5 (right) RPV.

For the POW rock a small amount of water is necessary to reach equilibrium in capillary pressure compared to the PWW rock. This is also reflected in the oil recovery profiles in Fig. 3 (right) after injecting a full reservoir pore volume (1 RPV). This demonstrates a key influence the capillary pressure has on the oil recovery of the system.

The influence of saturation functions will also be discussed in following sections through the *magnitude* of the capillary pressures, the role of viscosity ratio (appearing in $f$) and the Corey exponents, which all affect the time scale of imbibition through $D^m_{av}$.

3.2.2. *Distributions.* To illustrate the combined effect of advection and imbibition we present distributions of saturation and capillary pressure at different times in Fig. 5. Initially the water spreads into the reservoir in a bellshape. As the front travels further into the matrix the capillary pressure gradient at the fracture-matrix interface weakens and the imbibition rate goes down. Thus further down the fracture new imbibition fronts seemingly catch up with the old and a more uniform imbibition around the fracture develops. It is interesting to compare this model behavior with experimental results reported in [45] where CT images show a similar type of behavior for flow in, respectively, a gas-water and oil-water fracture-matrix system.

3.2.3. *Validation against full numerical model.* Before exploring the model further we want to check its validity by assessing the following two simplifications that have been made in the 1D+1D model:

A) Ignore terms related to viscous forces in the matrix ($\mathbf{v}^m_T = 0$ in model (7))
B) Ignore capillary pressure gradients in y-direction in the matrix (second term on RHS of (18))

We compare solutions from the 1D+1D model with solutions from the commercial simulator Eclipse 100 which solves the full 2D model. The same discretization was used ($N_x = 40, N_y = 120$). Eclipse solves the equations for saturations and pressures fully implicitly. Injector and producer wells are located in respectively the first and last fracture cell.

First, we check assumption A using the base case with POW curves. This set of curves allows low recovery by imbibition, but high recovery if the matrix is flooded efficiently by viscous forces. The permeability contrast $K_f/K_m$ was adjusted by varying $K_f$ in Eclipse. See Fig. 6.

Secondly, we check assumption B using the base case with PWW curves. We make variations in the factor $(L_x/L_y)^2$ appearing in (18) by reducing $L_y$ and $v^f_T$ (to keep the ratio $\tau^f = L_y/v^f_T$

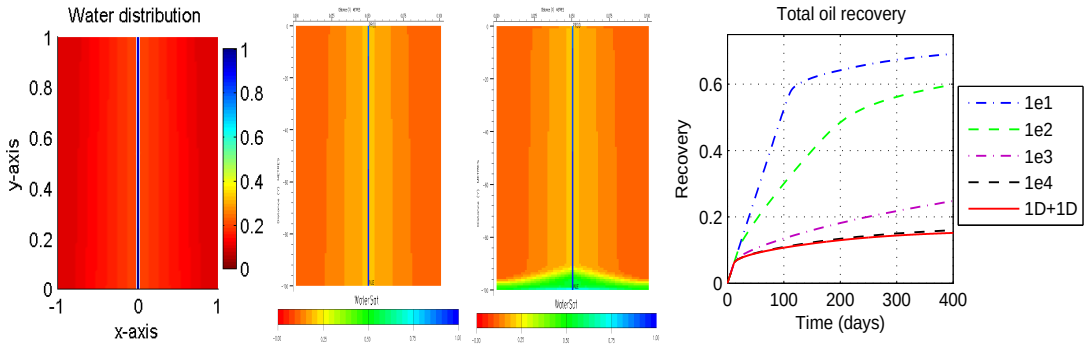


FIGURE 6. Left to right: Comparison of water distributions after 63 days (0.3RPV) from 1D+1D model, Eclipse with $K_f/K_m = 1e6$ and Eclipse with $K_f/K_m = 1e3$. Finally, recovery profiles from Eclipse with different $K_f/K_m$ and the 1D+1D model. Base case with POW curve set was used. Eclipse uses slightly different colors than the 1D+1D model.

constant). The solution of the 1D+1D model is then invariant since all scaled input parameters are the same. Results are presented in Fig. 7.

- For appropriate values of $K^f/K^m$ and $(L_x/L_y)^2$ the 1D+1D model and full 2D model give similar results as seen by water distribution (Pics. 1 and 2) and recovery (Pic. 4), respectively in Figs. 6 and 7.
- Viscous forces are significant in the matrix and lead to increased recovery as long as the permeability contrast $K_f/K_m$ is low, see Pic. 4 in Fig. 6. At $K_f/K_m \geq 1e4$ (in this case) the recovery from the matrix relies solely on imbibition and less oil is produced. In Pic. 3 of Fig. 6 both mechanisms are visible: the near-injector area is swept by viscous forces, while the area further downstream is produced by imbibition.
- If there is significant capillary flow parallel to the fracture the water can spread faster in the matrix than in the fracture: As illustrated in Pic. 3 of Fig. 7 the fracture water front lies well behind the water in the matrix. With less water positioned next to the saturated fracture (than if such flow was negligible) there is a stronger imbibition rate. This causes delayed breakthrough as seen in Fig. 7 by a longer linear profile in recovery (Pic. 4) and a shorter front length (Pic. 3) compared to the case where parallel flow is negligible (Pic. 1 and 2). The final recovery is however unaffected since it is limited by the imbibition potential.
- Only when $L_y$ is very close to $L_x$ does capillary flow parallel to the fracture become significant. That is attributed to the fact that the term in (18) is proportional to the square of $(L_x/L_y)$. Note also that if $\alpha$ was larger this term would be more significant.

3.2.4. *Parameter $\alpha$: Imbibition vs advection.* It was illustrated how capillary forces are important in terms of the saturation at which the capillary pressure vanishes. However, the magnitude of the capillary forces is also crucial for the efficiency of the imbibition process.

In order to demonstrate this the time scale of imbibition was varied in the base case by adjusting the parameter $P_{c,max}$ to produce different values of $\alpha$ (while keeping $\beta$ fixed), see (20). From Fig. 8 and 9 we observe:

- If the capillary forces are weak (small $\alpha$), the water will flow through the fracture while only the nearest matrix region is affected (left in Fig. 9). This is characterized by early water breakthrough as seen by the water front in the fracture (left in Fig. 8) and a low rate of oil production (middle in Fig. 8).
- If the capillary forces are strong (large $\alpha$), then the injected water is rapidly adsorbed into the matrix rather than flowing ahead along the fracture (middle and right in Fig. 9).

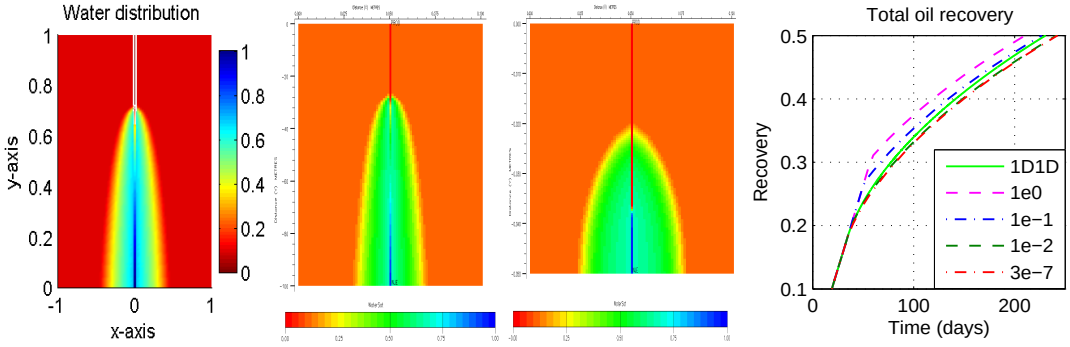


FIGURE 7. Left to right: Comparison of water distributions after 21 days (0.1 RPV) from 1D+1D model, Eclipse with $(L_x/L_y)^2 = 2.5e-7$ (base case) and Eclipse with $(L_x/L_y)^2 = 1$. Finally, recovery profiles from Eclipse with different $(L_x/L_y)^2$ and 1D+1D base case. Eclipse uses slightly different colors than the 1D+1D model.

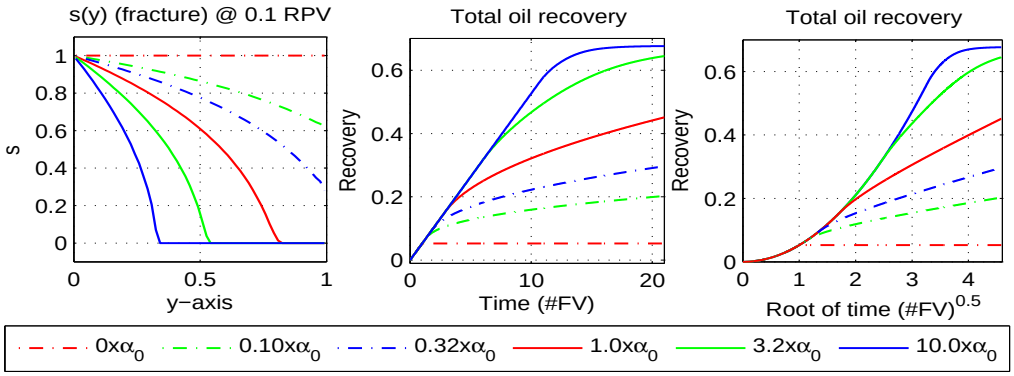


FIGURE 8. Impact of $\alpha$: The water front in the fracture (left) is more delayed with greater $\alpha$. The recovery profile is preferably linear vs time (middle) for large $\alpha$ and linear vs square root of time (right) for small $\alpha$ corresponding to the 'filling fracture' and 'instantly filled' regimes introduced in [45].

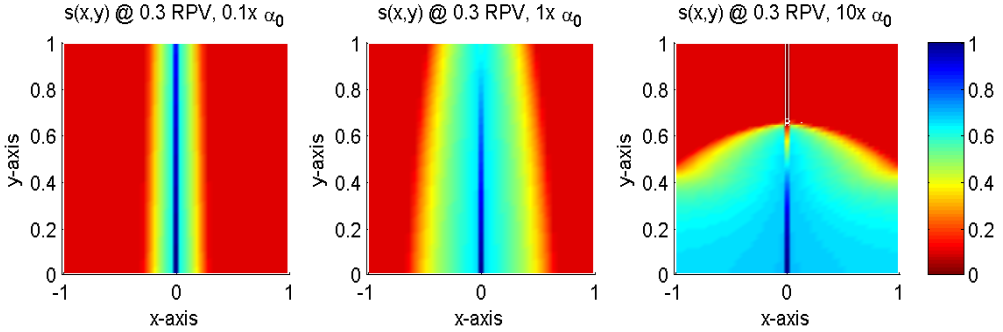


FIGURE 9. Distributions of water saturation at 0.3 RPV for low (left), reference (middle) and high (right) values of $\alpha$. If $\alpha$ is high, imbibition dominates over fracture flow and the water effectively displaces oil. For low $\alpha$ most of the water flows through the fracture without entering the matrix.

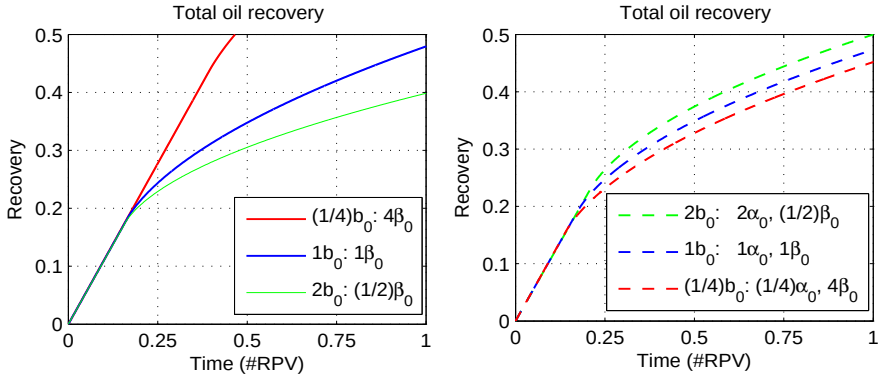


FIGURE 10. Sensitivity of $\beta$ in the base case. Left: Increased $\beta$ (at fixed $\alpha$) provides more efficient recovery. Right: Impact of fracture width $2b$ when rate is constant ($\alpha \cdot \beta$ fixed).

Strong imbibition therefore implies delayed breakthrough and a longer period of linear-profile recovery.

- The oil recovery curves in Fig. 8 (middle) are clearly composed of a linear part (vs. time #FV), and a nonlinear part. These two periods correspond to what is characterized as the "filling fracture" regime and the "instantly filled" regime in the work by Rangel-German and Kovscek [45]. We have plotted the oil recovery curves versus $\tau_f^{0.5}$ (right in Fig. 8) and we observe that the "nonlinear" part, the "instantly filled" regime, becomes approximately linear, as reported in [45]. The same authors also observed experimentally a more or less absent "filling fracture" regime for the water-oil system which can be explained by a small value of $\alpha$ in our model corresponding to weak capillary forces.
- In [52] a numerical sensitivity study was performed to describe vertically fractured reservoirs. A Peclet number (ratio of time scales for capillary diffusion and residence time) similar to $\alpha$ was found to be critical for evaluating the recovery efficiency.
- Reducing the rate will give the imbibition process more time per injected volume of water. In our model we note that a lower rate (given by $v_T^f$) increases $\alpha$, (see (20)). At a given amount of injected water ($\#\tau^f$) this results in higher recovery as seen in Fig. 8. Although in absolute time a low injection rate may take longer to achieve a given volume of water imbibed as compared to the high rate case, it represents a more efficient uptake of water by the matrix. We will later show (Section 3.2.7) that there is a minimum rate at which there is no benefit of further reduction.
- The rate-recovery phenomenon has also been reported in several experimental studies [32, 15, 45, 46]. Kleppe and Morse [32] observed in experiments that for a low and high rate case (differing by a factor of 10), that the low rate case was more efficient on a pore volume injected basis. Dutra and Aziz [15] later matched their experiments using a diffusion-type theory to model recovery by capillary imbibition.

3.2.5. *Parameter $\beta$: Adjusting the fracture width.* In this section we discuss the role of $\beta$. We can alter $\beta$ whereas $\alpha$ is kept fixed (see (20)) by altering the pore volume of the fracture. We keep the porosity at $\phi^f = 1$, but vary the width $2b$. If the matrix and fluid properties are fixed a constant $\alpha$ implies that $v_T^f$ remains constant. Then, assume we inject a certain volume of water into the reservoir. The speed is the same, but if the width has changed also the rate will differ. In the case of high $\beta$ (narrow fracture) the reservoir receives less water at a time and imbibition can work more efficiently. This is demonstrated in the recovery profiles for different $\beta$ in Fig. 10 (left). The time is measured in RPV (reservoir pore volumes) since 1 FV (fracture volume) is different in each case. For larger $\beta$ recovery is higher at a given injected volume. This behavior is also apparent

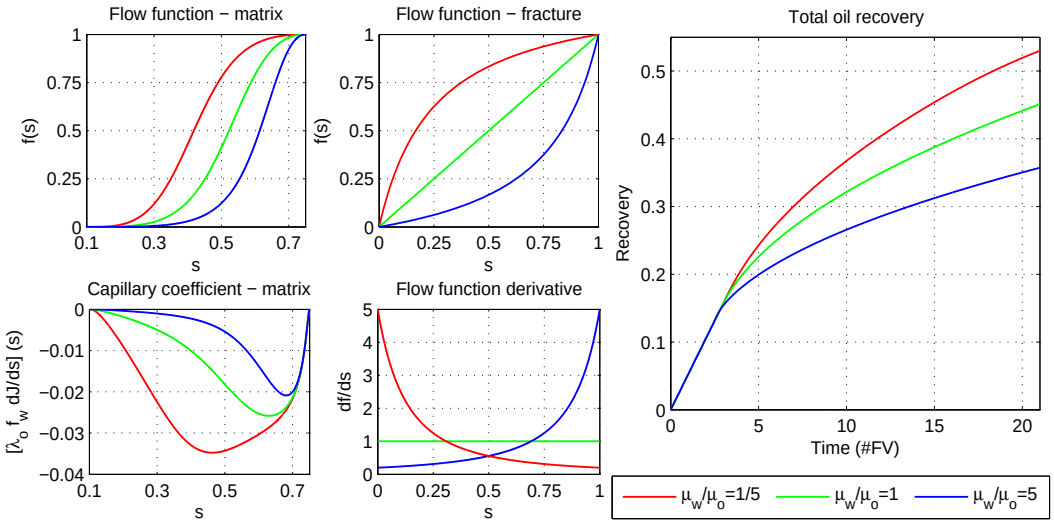


FIGURE 11. The effect of viscosity ratio $\mu_w/\mu_o$ on the base case (all other parameters are fixed): Fractional flow functions in matrix (top left) and fracture (top middle), the coefficient $\lambda_o^m f_w^m dJ/ds$ in matrix (down left) and the flow function derivative for the fracture (down middle). Low water viscosity (compared to oil viscosity) gives a more efficient oil recovery (right) due to improved imbibition.

from the the system (22) since $\beta$ relates to how much mass is transferred between the 2 systems. If $\beta$ is large we should expect the imbibition source term to be more important.

In Fig. 10 (right) results are shown for an example where the *injection rate* is kept constant whereas the width $2b$ of the fracture is varied with a factor $1/4$ and 2, respectively, relative to the base case. Clearly, a wider aperture gives a higher oil recovery. This was also observed experimentally in [45]. However, the difference between the three curves is not so large (as in the case where only $\beta$ was varied) due to the fact that a constant injection rate implies that $bv_T^f$ should be constant. Hence, a wider aperture $b$ implies that $\beta$ is reduced whereas $\alpha$ is increased as a consequence of a lower $v_T^f$.

3.2.6. *Viscosity ratio: adjusting water viscosity.* We want to determine the effect of viscosity ratio on the fracture-matrix flow. The oil viscosity is involved proportionally in the $\alpha$ parameter so we alter the *water viscosity* of the system. This only affects the flow functions in matrix and fracture, $f_w^m$ and $f_w^f$. We compare our reference example (with $\mu_w/\mu_o = 1$) to that of high and low viscosity ratio ($\mu_w/\mu_o$= 5 and 1/5).

- As seen from (6) and Fig. 11, decreasing the viscosity ratio $\mu_w/\mu_o$ generally increases the value of $f_w^m$, $f_w^f$. This correlation has primarily two consequences:
  - For low $\mu_w/\mu_o$ the water becomes more mobile compared to the oil and does not displace oil in the fracture as efficiently. In particular, low saturations will gain speed (as given by higher $f'(s)$).
  - The capillary diffusion coefficient $\lambda_o f_w J'$ increases (due to $f_w$) when lowering $\mu_w/\mu_o$. Reducing the viscosity of the imbibing water makes the imbibition process more efficient since the water flows easier.

  In an unfractured reservoir a high mobility ratio has a positive effect on recovery in the sense that water pushes the oil towards the producer in a piston-like manner resulting in late water breakthrough. In a fractured reservoir, one must also consider that increasing the water viscosity gives more resistance to spontaneous imbibition as given by a reduction in the capillary coefficient $\lambda_o f_w J'$.
- As seen from Fig. 12 (upper row) the saturation front in the fracture sharpens with higher viscosity ratio ($\mu_w/\mu_o = 5$) and smears more with lower ratio ($\mu_w/\mu_o = 1/5$). The front

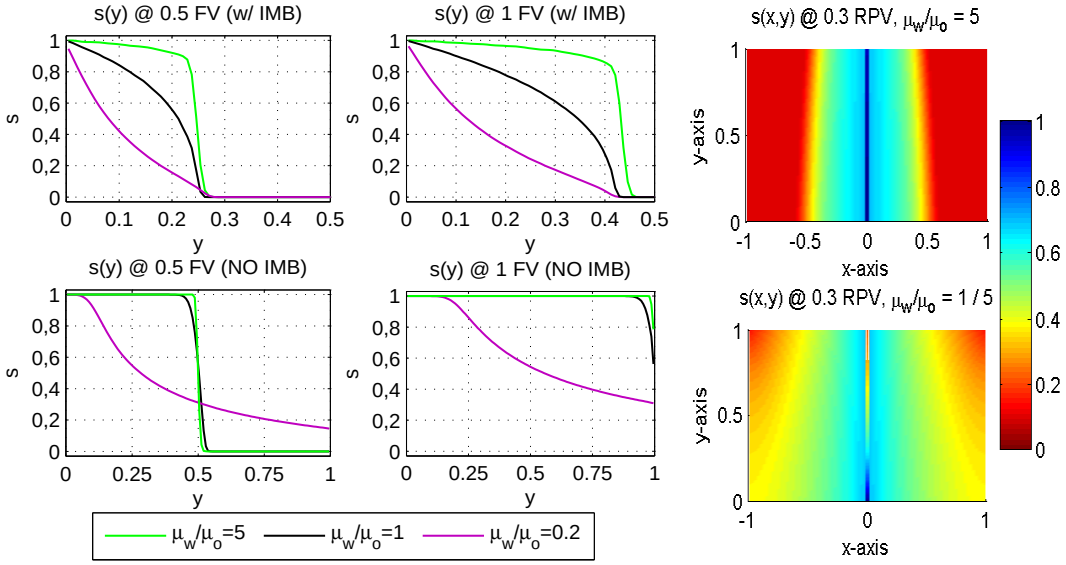


FIGURE 12. Sensitivity to viscosity ratio on the base case, while other parameters are kept fixed. The plots show water saturation in fracture after 0.5FV (left) and 1.0 FV (middle) and compare the profiles for different viscosity ratios ($\frac{\mu_w}{\mu_o} = 0.2, 1, 5$) when there is imbibition (top) and when not (below). The figures on the right show the distribution of water after 0.3 RPV for high viscosity ratio (top) and low (below).

is also smeared by the imbibition process: In the base case with neutral viscosity ratio $\mu_w/\mu_o = 1$ the smearing of the front is purely attributed to capillary imbibition (the case where imbibition is not included has a straight profile, see Fig. 12, lower row).

- It appears beneficial to use a low water viscosity: Although a low mobility ratio gives the water front in the fracture a high speed compared to the total velocity, the low front saturations are also the first to imbibe and this reduces the front speed considerably. Additionally, more of the water has imbibed in the case of lower viscosity ratios (Fig. 12, upper row). As a result, the front position in all 3 cases is approximately the same. This is a contrast to the situation without imbibition where oil is displaced more efficiently at high viscosity ratios and low saturations gain higher speeds when the viscosity ratio is reduced, see Fig. 12 (lower row).
- Also the recovery profiles in Fig. 11 (right) show that low water viscosity seems to be a good choice. In Fig. 12 (right) we illustrate saturation distributions after flooding 0.3 RPV of water. As seen, water imbibes faster into the matrix when the water viscosity is low.

3.2.7. *Characterizing numbers.* We have observed how recovery depends on some key parameters, like $\alpha, \beta$, capillary pressure and viscosities. To summarize we want to evaluate one number that can describe the overall behavior, a scaling number. Very simplified, water flows through the fracture with time scale $\tau^f$ and water imbibes into a matrix section with time scale $\tau^m$. There is $\beta\Delta s$ times as much volume of water that can imbibe into the matrix compared to the fracture volume. The ratio of time, denoted $\omega$, required to fill the matrix compared to the fracture should roughly be given as:

$$\omega = \tau^f / \Big(\frac{\tau^m}{\beta\Delta s}\Big) = \alpha\beta\Delta s. \tag{34}$$

In the following we test the hypothesis that $\omega = \alpha\beta\Delta s$ is a useful number to characterize the state of the system. We make a number of variations of the base case to obtain 5 different values of

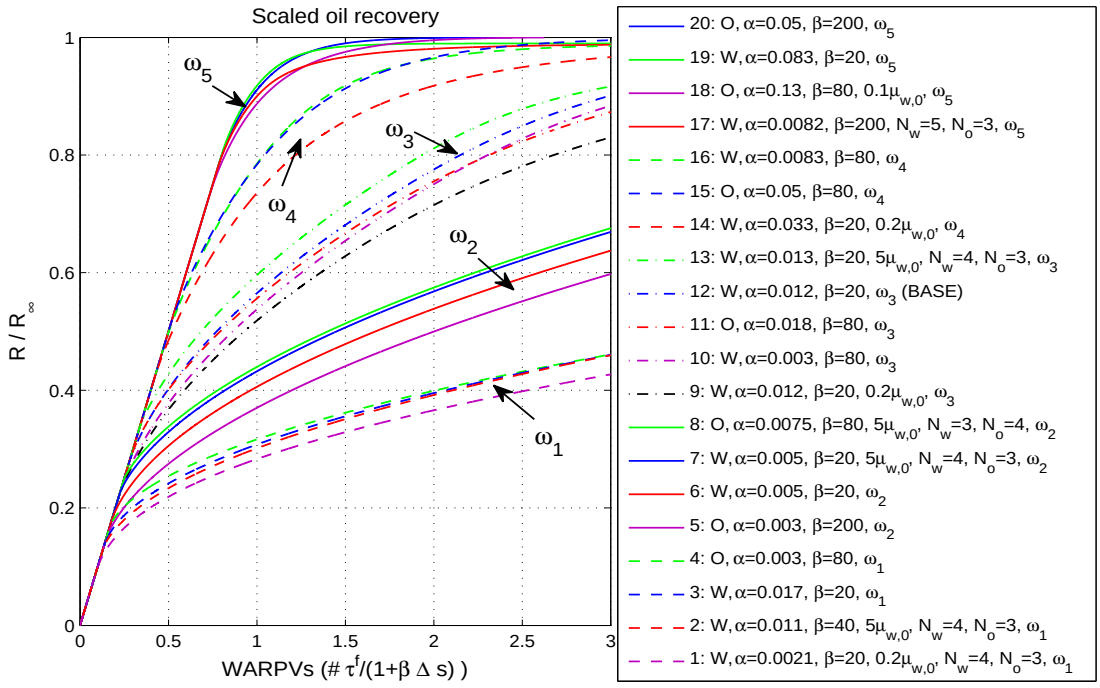


FIGURE 13. Obtainable recovery vs. water accessible pore volumes. Comparative test where $\omega = \alpha\beta\Delta s$ is constant for 5 values: $\omega_i$=0.025, 0.06, 0.15 (base), 0.4 and 1 ($i$=1,..,5). O and W denote POW and PWW sets. Parameters $\alpha$, $\beta$, $\Delta s$ are varied in 20 tests. $\omega$ seems to characterize the flow regime of the fracture-matrix system. Unspecified parameters are given by reference case.

omega: $\omega_1, \omega_2, ..., \omega_5$. For each fixed $\omega_i$ we vary parameters like $\alpha$, $\beta$, and saturation flow functions (POW, PWW) to take into account different flow scenarios. The values of $\omega$ differ roughly by a factor of 2.5 between adjacent groups. The results are shown in Fig. 13. For comparison the results are plotted as fraction of obtainable recovery, $R/R_\infty$ (where obtainable recovery is $R_\infty = \frac{1+\beta\Delta s}{1+\beta(1-s_0^m)}$) vs injected water-accessible reservoir pore volumes (WARPVs) ($\tau^f/(1+\beta\Delta s)$). The reason for this visualization is that if no water leaves until all possible imbibition has occurred and the fracture is full, the recovery will be $R/R_\infty = 1$ after 1 WARPV has been injected. This allows for direct comparison between different wetting states and volume ratios.

- The different simulations were performed with variations in fracture width, $P_{c,max}$, saturation curves (POW vs PWW), viscosity ratio and Corey exponents, resulting in different $\alpha$, $\beta$ and $\Delta s$. Curves with a given value of $\omega$ seem to overlap closely with little scattering.
- $\omega$ can be used quantitatively to describe the flow regime. The tests show that when $\omega \geq 0.4$ water imbibes very efficiently and breakthrough occurs after a large part of the obtainable oil has been produced. This corresponds to a dominant 'filling fracture' regime. When $\omega < 0.15$ the water spends much more time to imbibe than to fill the fracture. Water breakthrough occurs rapidly and a uniform imbibition occurs as described by the 'instantly filled' regime where most of the recovery profile follows a square root of time profile. For $0.15 < \omega < 0.4$ (roughly) a significant portion of water will imbibe before water breakthrough and a significant amount of recovery will be made after breakthrough (a mixture of the two regimes).
- It is not $\alpha$ alone that determines the flow regime. Cases 8, 16 and 17 have similar values of $\alpha$, but very different profiles. Also, considering cases 17-20 the profiles are similar, but the values of $\alpha$ very different.

- Varying viscosity ratio and Corey exponents affects the time scale for imbibition. As a nice illustration of how this is captured by $D_{av}$ consider first test 19 where a high $P_{c,max}$ in the reference case results in a high $\alpha$ (and $\omega = \omega_5 = 1$). Keeping this $P_{c,max}$ and increasing the water viscosity and Corey exponents until the calculated $\omega = \omega_3 = 0.15$ (base value) results in case 13 which fits well with the base case.
- The volume ratio affects the recovery regime. As seen by cases 4 vs. 5 and cases 15 vs. 20 where only the volume ratio is changed, the profiles end up in different regimes corresponding to the variation in $\omega$.
- The imbibition potential $\Delta s$ has a strong impact on the recovery regime. Given test 4 we changed curve set from POW to PWW to obtain test 10. Note that since $D_{av}^{pww} \approx D_{av}^{pow}$ (see (33)) we can consider both $\alpha$ and $\beta$ fixed. The change corresponds to a change in $\Delta s$ from 0.1 to 0.6 (and a factor of $6 \approx 2.5^2$ in $\omega$). As seen, the curves fell into different groups.
- At $\omega = 1$ most of the recovery profile is linear and further increasing $\omega$ would not offer significant improvement. Lower $\omega$ on the other hand quickly results in less efficient recovery. This result makes sense because if the time to imbibe the matrix takes longer than to fill the fracture ($\omega < 1$) it is more efficient to reduce the rate. If the time to imbibe is lower ($\omega > 1$), the matrix will be filled first, before the water breaks through. Using $\omega = 1$ can therefore be considered as an approximate criteria for the optimal injection rate in terms of efficiency. For the base case this could be achieved by lowering the rate by a factor of $\omega_5/\omega_3 \approx 7$ until 1.4m/d.
- In conclusion, $\omega$ seems to be a valid scaling number which incorporates time scales, volumes and imbibition potential. Note that we have only tested this numerically. Also, the scattering increased in cases where the diffusion coefficient was more nonlinear, which indicates that a more general scaling for $\tau^m$ could improve the match. Experimental validation should also be performed before drawing conclusions.

3.2.8. *An analytical fracture-matrix solution.* It is possible to draw some conclusions on the behavior of the system (21) and (22) as $\alpha \to \infty$. This means that the time scale for imbibition is much shorter than for advection. Let us denote this limit solution as $(s_\infty^f, s_\infty^m)$ and let $y^*(t)$ be the position of the water-front in fracture at time $t > 0$.

Consider the transport equation for the matrix, (21). Divide by $\alpha$ and let $\alpha \to \infty$. Then we get

$$\partial_x([\lambda_o^m f^m](s)\partial_x J^m(s)) = 0, \qquad (0 < x < 1; 0 < y < 1). \tag{35}$$

For flowing saturations $\lambda_o^m f_w^m > 0$, the conditions (35) and (30) imply a uniform capillary pressure along the x-axis for a given value of $y$, i.e. $J^m(s) =$ constant (with respect to space). Similarly, for the fracture model (22) we get the following condition on the fracture-matrix interaction

$$([\lambda_o f](s)\partial_x J(s))|_{x=0^+} = 0, \qquad (-(2/\beta) < x_f < 0; 0 < y < 1). \tag{36}$$

Now, let us consider a position $y$ along the fracture behind the water front, i.e., $y < y^*(t)$. Then, $[\lambda_o f_w](s) > 0$ and this implies in view of (35) and (36) that $J^f(s) = J^m(s) =$ constant $= 0$. Thus, $s = s_{eq}^m$. For $y \geq y^*(t)$, obviously, $s_\infty^f(y,t) = s_0^f$ and $s_\infty^m(x,y,t) = s_0^m$ where $s_0^f$ and $s_0^m$ are the initial saturations in fracture and matrix. This suggests the following matrix solution $s_\infty^m$ after a time $t > 0$:

$$s_\infty^m(x,y,t) = \begin{cases} s_{eq}^m, & y \in [0, y^*(t)); \\ s_0^m, & y \geq y^*(t), \end{cases} \qquad x \in [0,1], \tag{37}$$

where $s_{eq}^m$ is characterized by $J^m(s_{eq}^m) = 0$.

What remains is to determine the fracture saturation $s_\infty^f$ behind the front position $y^*(t)$ as well as the front position itself. In the construction of the solution we assume that the frontal fracture water (low saturations) is adsorbed by imbibition such that the matrix region is saturated behind the front. The solution can then be described by the Buckley-Leverett solution behind the front.

In the construction of the classical Buckley-Leverett solution the position should be placed such that mass conservation for the coupled fracture-matrix system is ensured. This gives the following

mass balance equations ($f = f^f$):

$$M^{\text{inj}} = \int_{s^f_{wr}}^{1-s^f_{or}} f'(\xi)t\, d\xi = [f(1-s^f_{or}) - f(s^f_{wr})]t. \tag{38}$$

In light of (37) the mass in the matrix region is given by

$$M^{\text{matrix}} = \beta y^*(t)(s^m_{eq} - s^m_0), \tag{39}$$

whereas the mass in the fracture region is given by (when it is constructed as a Buckley-Leverett solution where $s^*$ is a front at position $y^s$)

$$\begin{aligned} M^{\text{frac}} &= \int_{s^f_{wr}}^{1-s^f_{or}} y(s)\, ds = y^*(s^* - s^f_{wr}) + \int_{s^*}^{1-s^f_{or}} f'(s)t\, ds \\ &= f'(s^*)t(s^* - s^f_{wr}) + [f(1-s^f_{or}) - f(s^*)]t, \end{aligned} \tag{40}$$

where $s^*(t)$ is the front height in the fracture. Then, the mass balance $M^{\text{inj}} = M^{\text{matrix}} + M^{\text{frac}}$ gives the following relations for $s^*$:

$$f'(s^*) = \frac{f(s^*) - f(s^f_{wr})}{(s^* - s^f_{wr}) + \beta(s^m_{eq} - s^m_0)} \tag{41}$$

and $y^*(t) = f'(s^*)t$. Hence, the water saturation $s^f_\infty$ in the fracture is given by

$$s^f_\infty(y,t) = \begin{cases} s(y,t), & y \in [0, y^*(t)); \\ s^f_0, & y \geq y^*(t), \end{cases} \qquad x \in [0,1], \tag{42}$$

where $s \in [s^*, 1 - s^f_{or}]$ satisfies $f'(s)t = y$. Now we want to compare the numerical solution of the 1D+1D model for large values of $\alpha$ against the analytical solution given by (37) and (42).

- In the first example (left of Fig. 14) we consider the base case. Recall, we have used
$$s^f_{wr} = s^f_{or} = 0, \qquad s^f_0 = 0, \qquad s^m_0 = 0.1, \qquad s^m_{eq} = 0.7.$$
The flow function $f^f = s$ describes plug displacement and is given by a front over $s \in [0,1]$. Imbibition causes the front to be smoothed out and retained, but increased values of $\alpha$ makes the solution converge to a new front as predicted by the analytical solution. The front speed becomes $\frac{1}{1+\beta(s^m_{eq} - s^m_0)}$ (fracture lengths per injected FV) corresponding to a frontal displacement through the area water can displace and not just the fracture.
- In the second example we reduce $\beta$ to 4 (less volume for imbibition) and let $\mu_w/\mu_o = 1/5$ corresponding to a mobile water phase. See right plots in Fig. 14. This choice of parameters implies that the imbibition is less pronounced giving rise to an analytical solution which is composed of a front characterized by (41) and a rarefaction wave as in the classical Buckley-Leverett solution.

In both cases the 1D+1D solution seems to converge towards the predicted analytical solution as $\alpha$ becomes large. Especially, the correct front speeds and front saturations are reproduced. These two examples also verify that the numerical discretization of the 1D+1D model (21) and (22) as described in appendix C produce the correct solution.

**Remark 7.** *The problem for which we have constructed the analytical solution corresponds to a situation where the "filling fracture" regime is strongly dominating. An experimental observation of this regime is given in* [25] *where fractured blocks were flooded and the recovery profile was essentially linear. It is interesting to note that information about matrix properties are included in terms of two parameters: $\beta$ which characterizes the matrix pore volume divided by the fracture volume and the saturation $s^m_{eq}$ which represents the zero point of the matrix capillary pressure $P^m_c$, which in turn reflects information about the wetting state of the matrix. One should note that compared to the full system* (18) *large values of $\alpha$ also suggest more pronounced capillary flow parallel to the fracture (y-direction). The analytical solution is a good approximation if $\alpha(L_x/Ly)^2 << 1$ (to ensure negligible capillary flow in y-direction) at the same time as $\alpha >> 1$ (to ensure fracture filling regime).*

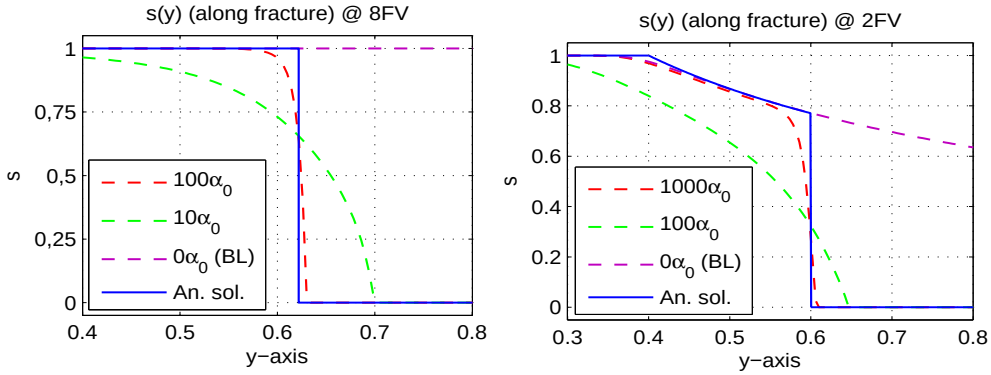


FIGURE 14. Comparison of numerical 1D+1D solution when $\alpha$ takes large values against analytical solution for $\alpha \to \infty$ and Buckley-Leverett. Left: base case with increased $\alpha$ after 8FV. Right: base case where $\beta = 4$ and $\mu_w/\mu_o = 1/5$ for increased $\alpha$ after 2FV.

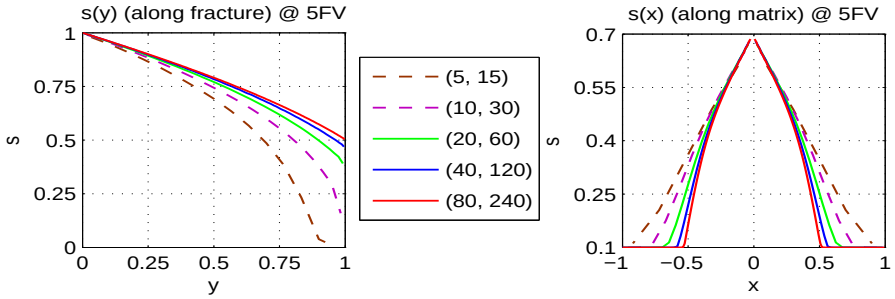


FIGURE 15. The effect of spatial discretization $(N_x, N_y)$ (where $N_x$ is number of blocks along positive x-axis and $N_y$ blocks along the y-axis) seen on the water front along fracture (left) and along matrix (right) at the center of the reservoir after 5FV. Base case was used.

3.2.9. *Sensitivity of numerical convergence.* Different discretizations of the grid were tested to evaluate the numerical accuracy. The reference case was tested where we compared dividing the x- and positive y-axis into $(N_x, N_y) = (5, 15), (10, 30), (20, 60), (40, 120)$ and $(80, 240)$ (both block dimensions are halved between every test). The results are compared in terms of the water front along the fracture and the imbibition front at the center of the reservoir after 5FV of water have been injected. Results in Fig. 15 show that the model behavior is sensitive to the spatial discretization: On a coarse grid the imbibition front goes deeper into the matrix, i.e. imbibition occurs on a shorter time scale. This numerically enhanced imbibition results in delayed front movement and delayed water breakthrough. The numerical error is negligible when using a discretization of $(20, 60)$ or finer. We have used $(40, 120)$ throughout.

We also consider the frequency of operator splitting. The base setting was 100 splitting steps per injected FV. This was checked by running the base case with splitting 100, 50, 25, 10 and 5 times per injected FV. Results are shown in Fig. 16. Notably, the numerical solutions seem very robust with respect to this numerical parameter. Even in the case of 5 splitting steps per FV the fracture solution seems to focus around the correct curve and the matrix imbibition profiles are undistinguishable. The profile along the fracture does however obtain a more step-like profile due to the less frequent interaction.

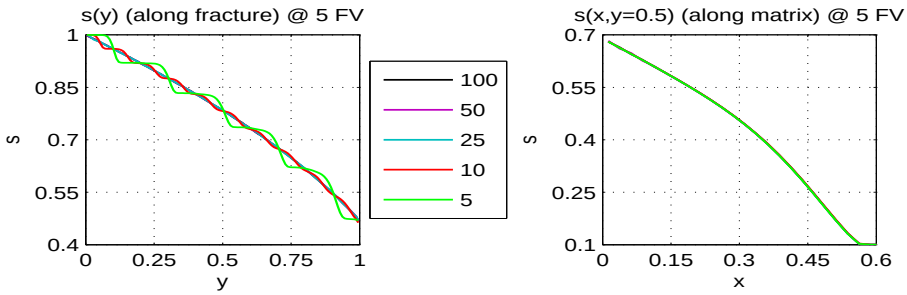


FIGURE 16. The effect of operator splitting frequency (# steps per injected FV) on the base case seen from water saturation profile along fracture (left) and along matrix (right) at the center of the reservoir after 5 FV.

## 4. Discussion and concluding remarks

A relatively simple and transparent 1D+1D fracture-matrix model has been formulated. The model was then used to demonstrate the role played by parameters like saturation functions, injection rate, volume of fractures vs. pore volume of matrix, different viscosity relations, and strength of capillary forces versus injection rate for flow in a fracture-matrix system. Two dimensionless variables, $\alpha$ and $\beta$, have been identified that clearly demonstrate the role played by the different physical parameters. A scaling number $\omega$ was suggested based on the parameters of the model that seems to correlate well with the regime of oil recovery. It is instructive to try to relate the model to previous works relevant for fracture-matrix flow. For example, an analytical solution for spontaneous imbibition has been discussed in the recent works [54, 55, 56]. A main feature of this solution is that it depends on a situation where the boundary condition is given in terms of a constant saturation, similar to a laboratory situation where the core plug is surrounded by a constant saturation. However, this is not the case in the 1D+1D model we consider. A key assumption in the construction of the 1D+1D model is that the fracture flow implies a varying fracture water saturation depending on the water injection rate and how much water that has been lost to the matrix through imbibition. Consequently, as remarked in [56] it is not so clear to what extent the results (the formulation of the analytical solution, the scaling, and the derivation of a transfer function) is directly relevant to a setting where the fracture saturation varies.

On the other hand, the 1D+1D model seems more relevant for a discussion of various fracture flow regimes (the "filling fracture" and "instantly filled" flow regime) as discussed in [47, 45, 19, 24, 16]. In particular, we also demonstrate (by numerical experiments) that the 1D+1D model will converge to a limit solution, which can be found analytically, when the time scale of the matrix imbibition becomes small, i.e., the "filling fracture" regime becomes dominating. This represents the opposite situation of that considered in [31] and also discussed in works like [12, 60], where analytical solutions are derived when it is assumed that the fracture is quickly filled with water (the instantly filled regime).

In [12] the authors investigate a dual-porosity model formulation based on using streamlines. The fracture dominated advective flow is described by 1-D transport along streamlines whereas fracture-matrix transfer is represented by a source or sink term. The matrix model is given in terms of an ODE equation which involve a representative saturation (similarly for a concentration of the reactive agent) for the matrix region. Linear transfer functions similar to (1) were derived based relying on ideas used in [31]. Analytical solutions valid at early times and late times respectively, are then derived and compared to the numerical solutions based on a discretization of the fracture-matrix model. A main difference between this approach and the 1D+1D model we discuss is that we consider a PDE to represent the imbibition from the matrix region instead of a transfer term generated from an ODE equation. The main motivation is to ensure that more details about the imbibition process (how it develops in space and time) are taken into account.

However, one might envision that we could employ the reduced 1D+1D model and test different transfer functions like those that have been developed in [12, 31].

In the work [21] the authors develop a multi-rate mass transfer model for two-phase fracture-matrix flow in a complex geometry. The fracture model includes viscous forces and gravity whereas the flow in matrix is assumed to be controlled by capillary forces only. It is assumed that fluid transfer between fracture and matrix and flow in the matrix is due to capillary diffusion only. In that sense the 1D+1D model we discuss is similar. However, in [21] the diffusion model is based on a constant diffusion equation (obtained by an averaging of the nonlinear capillary diffusion coefficient). Hence, the matrix behavior is given in terms of a semi-analytical solution which allows the authors to simulate a wide range of transfer rates, early time as well as late time behavior. However, one might expect that some effects are ignored due to the use of a constant diffusivity constant.

As a final remark we mention that the 1D+1D model could be a possible tool to evaluate laboratory experiments in simpler geometries where focus is on a more detailed description of the fracture-matrix interaction [19, 24, 45, 46]. The model is simple enough to allow for more qualitative understanding, as reflected by the construction of the analytical solution for the limiting case when $\alpha \to \infty$. The formulation of the fracture-matrix model and the approach used to solve it allow us to, in a next phase, take into account effects from fluid-rock chemistry. Preliminary versions of such models have been developed for interpretation of brine-dependent spontaneous imbibition experiments on core plugs [4, 18, 26, 63, 66]. However, these models are rather complicated as they involve a coupling between the water-oil transport model and a transport-reaction model which is able to describe fluid-rock chemistry for seawater-like brines in chalk. In particular, a number of different ions and minerals must possibly be taken into account. The proposed fracture-matrix model studied in this work represents a possible framework for systematic studies of certain aspects of such coupled systems, at least for idealized fracture-matrix systems.

## Appendix A. Matrix capillary pressure

A.1. **A family of capillary pressure curves.** Mixed-wet capillary pressure data is typically asymmetric around the s-axis and the crossing point depends on the wettability of the system. As a representation, consider the function

$$J^m(s^*) = \frac{a_1}{1+k_1 s^*} - \frac{a_2}{1+k_2(1-s^*)} + b, \qquad s^* = \frac{s - s_{wr}}{1 - s_{or} - s_{wr}}. \tag{43}$$

$J$ is monotonously decreasing and bounded (in function and derivative) if the parameters $a_1, a_2, k_1, k_2$ are nonnegative. Let the endpoints be given such that $J^m(0) = A$ and $J^m(1) = B$, where $A > B$ since $J$ is decreasing. Then the parameters $a_1, a_2$ are given as

$$a_1 = (A-b) + (A-b)\frac{1}{((1+k_2)(1+k_1)-1)} + (b-B)\frac{(1+k_1)}{((1+k_2)(1+k_1)-1)}, \tag{44}$$

$$a_2 = (A-b)\frac{1+k_2}{((1+k_2)(1+k_1)-1)} + (b-B)\frac{(1+k_2)(1+k_1)}{((1+k_2)(1+k_1)-1)}. \tag{45}$$

We see that $a_1, a_2 \geq 0$ if $A \geq b \geq B$. The 5 parameters $A, B, k_1, k_2, b$ can be used to match experimental capillary pressure data. $A, B$ represent the endpoints at residual saturations. There are then 3 free shape parameters to fit the remaining data. Especially, $k_1$ and $k_2$ control the gradient at low and high saturations respectively while $b$ has more effect on the level of the intermediate part of the curve.

A.2. **Parameters for capillary pressure and relative permeability.** Different curves are represented by different choices of function parameters. We assume that $J$ is normalized to the maximum capillary pressure in the system so that $J$ does not exceed $\pm 1$. These extremes are set at the critical saturations. Therefore $A = -B = 1$. The chosen set of parameters for PWW and POW matrix are given in Table 2.

| | $A$ | $B$ | $k_1$ | $k_2$ | $b$ | | $k_w^*$ | $N_w$ | $k_o^*$ | $N_o$ | | $s_{wr}$ | $s_{or}$ |
|---|---|---|---|---|---|---|---|---|---|---|---|---|---|
| Pref. oil-wet | 1 | -1 | 30 | 40 | -0.22 | | 0.7 | 2.0 | 0.75 | 3.0 | | 0.10 | 0.15 |
| Pref. water-wet | 1 | -1 | 30 | 50 | 0.20 | | 0.4 | 3.0 | 0.9 | 2.0 | | 0.10 | 0.25 |

TABLE 2. Input parameters for matrix scaled capillary pressure function $J^m$ and for relative permeability curves $k_{rw}, k_{ro}$. A set of parameters is defined for each wetting state: preferentially oil-wet or preferentially water-wet.

## APPENDIX B. OPERATOR SPLITTING

We will rely on a numerical approach in order to resolve the coupled system (21)-(22). More precisely, we shall employ an operator splitting approach where the scaled transport system (21)-(22) is split into the following two subsystems accounting respectively for viscous transport and capillary driven mass distribution:

- System 1: *Flow in the y-direction*

$$\begin{aligned} \partial_t s_w &= 0, && (0<x<1; 0<y<1); \\ \partial_t s_w + \partial_y f_w^f &= 0, && (-(2/\beta)<x_f<0; 0<y<1). \end{aligned} \tag{46}$$

  When capillary forces are neglected it follows that changes are related to advective flow in the y-direction only. Hence, the state of the matrix is kept fixed, while the fracture state changes.

- System 2: *Flow in the x-direction*

$$\begin{aligned} \partial_t s_w &= -\alpha \partial_x(\lambda_o^m f_w^m \partial_x J^m), && (0<x<1; 0<y<1); \\ \partial_t s_w &= -\alpha\beta\Big(\lambda_o^m f_w^m \partial_x J^m\Big)^m|_{x=0^+} && (-(2/\beta)<x_f<0; 0<y<1). \end{aligned} \tag{47}$$

  For this case all changes are driven by capillary forces. The entire system changes in time, but only by flow in x-direction.

For a fully discrete scheme where we solve (46) and (47) in separate steps, we refer to Appendix C. Note that the above splitting approach corresponds to the so-called dimensional splitting method commonly used to solve a multi-dimensional problem as a series of one-dimensional problems [33].

## APPENDIX C. NUMERICAL DISCRETIZATION AND STABILITY ANALYSIS

In the following we describe the discrete schemes used to solve numerically the two subsystems (46) and (47).

### C.1. System 1: fracture flow given by (46).

The fracture flow system below

$$\partial_t s_w + \partial_y f_w^f = 0, \qquad (-2/\beta < x_f < 0; 0<y<1) \tag{48}$$

is discretized (skipping the 'w' and 'f' indices) in the following manner

$$\frac{s_i^{n+1}-s_i^n}{\Delta t} + \frac{f_{i+1/2}-f_{i-1/2}}{\Delta y} = 0 \qquad (i=1,...,Ny). \tag{49}$$

We will use a similar approach as described in [66] to evaluate the fluxes at the cell boundaries. Define the terms

$$f^+(s_i) := f(s_i) + \nu^{1/2} s_i, \qquad f^-(s_i) := f(s_i) - \nu^{1/2} s_i. \tag{50}$$

Then we get a first order approximation in $\Delta x$ by letting

$$f_{i+1/2} := 1/2[f^+(s_i) + f^-(s_{i+1})]. \tag{51}$$

By backsubstitution we see that this choice corresponds to a combination of a central discretization of $f$ and a diffusive term where $\nu^{1/2}$ plays the role of a numerical viscosity.

$$s_i^{n+1} - s_i^n = -\frac{\Delta t}{\Delta y}\Big[\frac{f(s_i)+f(s_{i+1})}{2} - \frac{f(s_{i-1})+f(s_i)}{2}\Big] + \nu^{1/2}\frac{\Delta t}{\Delta y}\Big[\frac{s_{i+1}-2s_i+s_{i-1}}{2}\Big]. \tag{52}$$

The diffusive part has the role of smoothing out fronts and thus limits the gradients, but for fixed $\frac{\Delta t}{\Delta y}$ the diffusion goes to zero with refinement such that the scheme is consistent.

Second order approximation in $\Delta y$ is found using the MUSCL scheme. That is incorporated by adjusting the term $f_{i+1/2}$ as follows

$$f_{i+1/2} := \frac{1}{2}\Big[f^+(s_i) + \frac{\Delta y}{2}\sigma_i^+\Big] + \frac{1}{2}\Big[f^-(s_{i+1}) - \frac{\Delta y}{2}\sigma_{i+1}^-\Big] \tag{53}$$

where $\sigma^\pm$ represent a gradient in $f$. They are evaluated such that $\sigma_i^+ = \sigma(\delta f_{i-1/2}^+, \delta f_{i+1/2}^+)$ and $\sigma_{i+1}^- = \sigma(\delta f_{i+1/2}^-, \delta f_{i+3/2}^-)$ where

$$\delta f_{i+1/2}^+ = \frac{1}{\Delta y}(f^+(s_{i+1}) - f^+(s_i)), \qquad \delta f_{i+1/2}^- = \frac{1}{\Delta y}(f^-(s_{i+1}) - f^-(s_i)) \tag{54}$$

and $\sigma$ is chosen to be the Superbee slope limiter function:

$$\sigma(u,v) = \frac{sgn(u) + sgn(v)}{2} \cdot \max\Big(\min(2|u|, |v|), \min(|u|, 2|v|)\Big). \tag{55}$$

C.1.1. *Stability.* For a stable discretization of the given scheme(s) we must have sufficient numerical diffusion and small enough time step. Then we choose $\nu$ such that $\nu - f'(s)^2 \geq 0$ for any relevant $s$ (see [66] for details). Choosing $\nu$ too large will however smear out the solution so the optimal choice is to set $\nu = \sup_s (f'(s))^2$ for the relevant range of $s$. Regarding the time step we use the following CFL-condition: $\sup_s |f'| \frac{\Delta t}{\Delta y} < 0.5$ associated with a standard forward Euler discretization in time.

C.1.2. *Boundaries.* At the injector boundary of cell 1 we use the information of the injected fluid as given by $s_{inj}$. We therefore set $f_{1/2} = f(s_{inj})$. At the producer boundary we assume the flux out is given by the last cell only such that $f_{Ny+1/2} = f(s_{Ny})$.

C.2. **System 2: Capillary flow in the matrix given by** (47)**.** We recall the scaled form of the system with exclusively capillary flow:

$$\begin{aligned} \partial_t s &= -\alpha \partial_x(\lambda_o^m f_w^m \partial_x J^m), && (0 < x < 1; 0 < y < 1); \\ \partial_t s &= -\alpha\beta\Big(\lambda_o^m f_w^m \partial_x J^m\Big)|_{x=0^+}, && (-2/\beta < x_f < 0; 0 < y < 1). \end{aligned} \tag{56}$$

This system is convenient to consider relatively the dimensionless time $t^* = \frac{t}{\tau^m}$, i.e. $\frac{t^*}{t'} = \alpha$ where $t'$ is given in (15). Consequently, the model (56) relatively $t^*$ (where we skip the $^*$ superscript) takes the form

$$\begin{aligned} \partial_t s &= -\partial_x(\lambda_o^m f_w^m \partial_x J^m), && (0 < x < 1; 0 < y < 1); \\ \partial_t s &= -\beta\Big(\lambda_o^m f_w^m \partial_x J^m\Big)|_{x=0^+}, && (-2/\beta < x_f < 0; 0 < y < 1). \end{aligned} \tag{57}$$

The fracture is connected with the matrix by letting the fracture be cell 1 in the grid we consider and then let cells $2, ..., N_x + 1$ cover the $N_x$ cells of the matrix with the lowest numbers corresponding to cells closest to the fracture.

At first, we consider the discretization of the first equation of (57) in the interior domain of the matrix (first equation):

$$\frac{s_i^{n+1} - s_i^n}{\Delta t} = -\frac{(\lambda_o^m f_w^m)_{i+1/2}\frac{J_{i+1}^m - J_i^m}{\Delta x} - (\lambda_o^m f_w^m)_{i-1/2}\frac{J_i^m - J_{i-1}^m}{\Delta x}}{\Delta x} \qquad (i = 3, ..., N_x). \tag{58}$$

We need to evaluate the coefficients at the boundaries by means of an appropriate averaging. It can be seen by inspecting the equations that a cell receives water from another if it has higher capillary pressure (since the coefficients are nonnegative). We want to shape the coefficients so that water does not move from a cell with residual water saturation and does not enter a cell (thus displacing oil) with residual oil saturation. This is accomplished by the choice of an upwind formulation, in the sense that the coefficients depend on the direction of which the flow of water is going:

$$(\lambda_o f)_{i+1/2} = [(\lambda_o)_{i+1} f_i] \max\{0, \text{sign}(J_{i+1} - J_i)\} + [(\lambda_o)_i f_{i+1}] \max\{0, -\text{sign}(J_{i+1} - J_i)\}. \tag{59}$$

Consequently, the following features are ensured to hold:

- If $J_{i+1} > J_i$: In this case $(\lambda_o f)_{i+1/2} = (\lambda_o)_{i+1} f_i$ and so water leaves from cell $i$ to $i+1$ if $i$ has more than residual water and $i+1$ has more than residual oil.
- If $J_{i+1} < J_i$: In this case $(\lambda_o f)_{i+1/2} = (\lambda_o)_i f_{i+1}$ and water leaves $i+1$ to $i$ if $i+1$ has more than residual water and $i$ has more than residual oil.

At the first cell in matrix region we have the following scheme:

$$\frac{s_2^{n+1} - s_2^n}{\Delta t} = -\frac{(\lambda_o^m f^m)_{5/2} \frac{J_3^m - J_2^m}{\Delta x} - (\lambda_o f)_{3/2} \frac{J_2^m - J_1^f}{\Delta x/2}}{\Delta x}, \qquad i = 2, \tag{60}$$

where we have used that $\partial_x J^m|_{x=0^+} \approx \frac{J_2^m - J_1^f}{\Delta x/2}$. At the last cell we can assume a closed boundary such that $(\lambda_o f)_{N_x+3/2} = 0$ or we can assume a symmetric system beyond this point. In that case $\frac{J_{N_x+2} - J_{N_x+1}}{\Delta x} = 0$ and the result is the same: a zero flux across the boundary.

$$\frac{s_{N_x+1}^{n+1} - s_{N_x+1}^n}{\Delta t} = -\frac{0 - (\lambda_o^m f^m)_{N_x+1/2} \frac{J_{N_x+1}^m - J_{N_x}^m}{\Delta x}}{\Delta x}, \qquad (i = N_x + 1). \tag{61}$$

Regarding the discretization of the fracture cell represented by the second equation of (57) we have

$$\frac{s_1^{n+1} - s_1^n}{\Delta t} = -\beta (\lambda_o f)_{3/2} \frac{J_2^m - J_1^f}{\Delta x/2}, \qquad (i = 1). \tag{62}$$

This is consistent with the discretization in (60) of the flux at the interface between fracture and matrix.

C.2.1. *Stability.* For simplicity reasons we employ a forward Euler discretization in time. For stability we require that the capillary pressure does not oscillate as it is supposed to behave in a diffusive manner and drive the changes in saturations. Water will flow towards higher capillary pressure and decrease the capillary pressure as a consequence. But if so much water is transported during a time step that the capillary gradient changes, then water will flow back where it came from and this is observed as oscillations in both saturation and capillary pressure.

Consider 3 adjacent cells $i-1$, $i$, $i+1$ in the matrix. The capillary pressure in cell $i$ should not change more from one time step to the next than half of the maximum difference in capillary pressure between $i$ and the neighbor cells. Then no adjacent points will ever pass each other in terms of capillary pressure.

$$\begin{aligned}
|J(s_i^{n+1}) - J(s_i^n)| &\leq |J'(s)|_{max} |s_i^{n+1} - s_i^n| \\
&= |J'(s)|_{max} \frac{\Delta t}{\Delta x} |(\lambda_o f \partial_x J)_{i+1/2} - (\lambda_o f \partial_x J)_{i-1/2}| \\
&\leq |J'(s)|_{max} \frac{\Delta t}{\Delta x^2} 2 \max(\lambda_o f) \max(|J_{i+1} - J_i|, |J_i - J_{i-1}|) \\
&\leq \frac{1}{2} \max(|J_{i+1} - J_i|, |J_i - J_{i-1}|).
\end{aligned}$$

In conclusion this leads to $\Delta t \leq \frac{\Delta x^2}{4(\lambda_o f)_{max} |(J^m)'(s)|_{max}}$. A similar derivation at the matrix-fracture transition yields a stability criterion of the form: $\Delta t \leq \frac{\min(\frac{2}{\beta}, \Delta x) \frac{\Delta x}{2}}{4(\lambda_o f)_{max} (|(J^f)'|, |(J^m)'|)_{max}}$.

## References


[1] S. Akin, J.M. Schembre, S.K. Bhat, A.R. Kovscek, Spontaneous imbibition characteristics of diatomite, *J. Pet Sci Eng*, **25**, pp. 149-165, 2000.

[2] B. Agarwal, H. Hermansen , J.E. Sylte, L.K. Thomas, Reservoir Characterization of Ekofisk Field: A Giant, Fractured Chalk Reservoir in the Norwegian North Sea - History Match , *SPE Res Eval & Eng* **3** (6), 534–543, 2000.

[3] W.M. Ahr, Geology of Carbonate Reservoirs, John Wiley and sons, 2008.

[4] P.Ø. Andersen, S. Evje, M.V. Madland, and A. Hiorth, A geochemical model for interpretation of chalk core flooding experiments, *Chem. Eng. Sci.*, **84**, pp. 218–241, 2012.

[5] P.Ø. Andersen and S. Evje, Two-phase flow in a fissurized-porous media, *AIP Conf. Proc.*, **1479**, pp. 2340, 2012.
[6] W.G. Anderson, Wettability Literature Survey-Part 4: Effects of Wettability on Capillary Pressure, *J. Pet Tech* **39** (10), pp. 1283–1300, 1987.
[7] W.G. Anderson, Wettability Literature Survey Part 5: The Effects of Wettability on Relative Permeability, *J. Pet Tech* **39** (11), pp. 1453–1468, 1987.
[8] H. Behbahani and M.J. Blunt, Analysis of Imbibition in Mixed-Wet Rocks Using Pore-Scale Modeling, *SPE J.* **10** (4), pp. 466–474, 2005.
[9] R.H. Brooks and A.T. Corey, Hydraulic properties of porous media, *Hydrological Papers (Colorado State University)* **3**, 1964.
[10] S-E. Buckley and M. Leverett, Mechanism of fluid displacement in sand, *Trans. AIME*, **146**, pp. 107, 1942.
[11] M. Cil, J.C. Reis, A multi-dimensional, analytical model for counter-current water imbibition into gas-saturated matrix blocks, *J. Pet. Sci. Eng.*, **16**, pp. 61-69, 1996.
[12] G. DiDonato and M.J. Blunt, streamline-based dual porosity simulation of reactive transport and flow in fractured reservoirs, *Water Res. Res.*, **40**, 2004.
[13] A.B. Dixit, S.R. McDougall, K.S. Sorbie, J.S. Buckley, Pore-Scale Modeling of Wettability Effects and Their Influence on Oil Recovery, *SPE Res Eval & Eng*, **2** (1), 25–36, 1999.
[14] J. Douglas, T. Arbogast, P.J. Paes-Leme, J.L. Hensley, N.P. Nunes, Immiscible displacement in vertically fractured reservoirs, *Tran. Por. Med.*, **12**, 73–106, 1993.
[15] T.V. Dutra and K. Aziz, A new double-porosity reservoir model for oil/water flow problems, *SPE Res Eng*, 419-425, 1992.
[16] M. Dejam and H. Hassanzadeh, Formation of liquid bridges between porous matrix blocks, *AIChE Journal*, **57** (2), 286–298, 2010.
[17] A. Firoozabadi, Recovery mechanisms in fractured reservoirs and field performance, *JCPT*, **39** (11), 13–17, 2000.
[18] S. Evje, A. Hiorth, *A model for interpretation of brine-dependent spontaneous imbibition experiments*, Adv. Water Resources, **34**(12), 1627–1642, 2011.
[19] M.A. Fernø, A. Haugen and A. Graue, Wettability effects on the matrix-fracture fluid transfer in fractured carbonate rocks, *J. Pet Sci Eng*, **77** (1), pp. 146–153, 2011.
[20] P.S. Gautam and K.K. Mohanty, Matrix-fracture transfer through countercurrent imbibition in presence of fracture fluid flow, *Tran. Por. Med.* **55**, 309–337, 2004.
[21] S. Geiger, M. Dentz, I. Neuweiler, A novel multi-rate dual porosity model for improved simulation of fractured and multi-porosity reservoirs, *SPE J.*, 2013.
[22] A. Graue, T. Bognø, B.A. Baldwin and E.A. Spinier, Wettability effects on oil-recovery mechanisms in fractured reservoirs, *SPE Res Eval & Eng* **4** (6), pp. 455–465, 2001.
[23] L.D. Hallenbeck, J.E. Sylte, D.J. Ebbs, L.K. Thomas, Implementation of the Ekofisk Field Waterflood, *SPE Form Eval* **6** (3), 284–290, 1991.
[24] Å. Haugen, M.A. Fernø, A. Graue, Comparison of numerical simulations and laboratory waterfloods in fractured carbonates, *Presented at SPE Annual Technical Conference 2007 California, USA*, Nov 2007.
[25] A. Haugen, M.A. Fernø, Ø. Bull, A. Graue, Wettability Impacts on Oil Displacement in Large Fractured Carbonate Blocks, *Energy & Fuels* **24**, 3020–3027, 2010.
[26] A. Hiorth, L.M. Cathles, and M.V. Madland, The Impact of Pore Water Chemistry on Carbonate Surface Charge and Oil Wettability, *Transport Porous Media* **85**, 1–21, 2010.
[27] , H. Hotetot and A. Firoozabadi, An efficient model for incompressible two-phase flow in fractured media, *Adv. Water Resour.* **31**, pp. 891–905, 2008.
[28] R.G. Hughes, M.J. Blunt, Network modeling of multiphase flow in fractures, *Adv. Water Resour.*, **24** (3-4), pp. 409421, 2001.
[29] M. Karimi-Fard, L.J. Durlofsky, K. Aziz, An efficient discrete-fracture model applicable for general purpose reservoir simulators, *SPE J.* **9**, pp. 227–236, 2004.
[30] D. Kashchiev and A. Firoozabadi, Analytical solutions for 1D countercurrent imbibition in water-wet media, *SPE J.*, **8** (4), 401–408, 2003.
[31] H. Kazemi, J.R. Gilman, and A.M. Elsharkawy, Analytical and numerical solution of oil recovery from fractured reservoirs with empirical transfer functions, *SPE Res Eng*, **Vol 6**, 219–227, 1992.
[32] J. Kleppe and R.A. Morse, Oil production from fractured reservoirs by water displacement, in *Proceedings of the Annual Meeting of the Society of Petroleum Engineers*, paper SPE 5084, Soc. of Pet. Eng., Richardson, Tex., 1974.
[33] R.J. LeVeque, Finite Volume Methods for Hyperbolic Problems, Cambridge Texts in Applied Mathematics, Berlin, 2002.
[34] F. Lomeland and E. Ebeltoft, A new versatile Capillary Pressure Correlation, *International symposium of the Society of Core Analysts, Abu Dhabi, UAE*, 29 Oct - 2 Nov, 2008.
[35] M. Mainguy and F.-J. Ulm, Coupled diffusion-dissolution around a fracture channel: The solute congestion phenomenon, *Tran. Por. Med.* **80**, 481–497, 2001.
[36] S.K. Masalmeh, and I.A. Shiekah and X.D. Jing, Improved Characterization and Modeling of Capillary Transition Zones in Carbonate Reservoirs, *SPE Res Eval & Eng* **10** (2), 191–204, 2007.

[37] S.K. Matthi, A. Mezentsev, and M. Belayneh, Finite-element node-centered finite-volume experiments with fractured rock represented by unstructered hybrid element meshes, *SPE Res Eval & Eng.* **10**, pp. 740–756, 2007.
[38] D. McWhorter, D. Sunada, Exact Integral Solutions for Two-Phase Flow, *Water Resour. Res.*, **26** (3), pp. 399-413, 1990.
[39] K. Mogensen, E.H. Stenby, A dynamic two-phase pore-scale model of imbibition, *Transp. Porous Media*, **32**, pp. 299-327, 1998.
[40] I. Palaz and K.J. Marfurt, Carbonate seismology, Society of Exploration Geophysicists, 1997.
[41] X. Pan and R.C. Wong, Steady state two-phase in a smooth parallel fracture, Ann. Tech. Meeting of the Petroleum Society in Calgary, Alberta, Canada, June 10 12, 1996.
[42] P. Persoff and K. Pruess, Two-phase flow visualization and relative permeability measurement in natural rough-walled rock fractures, *Water Resour. Res.*, **31**, pp. 11751186, 1995.
[43] M. Pooladi-Darvish and A. Firoozabadi, Cocurrent and countercurrent imbibition in a water-wet matrix block, *SPE J.*, **5** (1), 3–11, 2000.
[44] E.R. Rangel-German, S. Akin, L. Castanier, Multiphase-flow properties of fractured porous media, *J. Pet. Sci. Eng.*, **51**, (3-4), 197–213, 2006.
[45] E.R. Rangel-German and A.R. Kovscek, Experimental and analytical study of multidimensional imbibition in fractured porous media, *J. Pet. Sci. Eng.*, **36**, 45-60, 2002.
[46] E.R. Rangel-German and A.R. Kovscek, A micromodel investigation of two-phase matrix-fracture transfer mechanism, *Water Res. Res.*, **42**, pp. 1–13, 2006.
[47] E.R. Rangel-German and A.R. Kovscek, Time-dependent matrix-fracture shape factors for partially and completely immersed fractures, *J. Pet. Sci. Eng. Sci.*, **54**, pp. 149–163, 2006.
[48] V. Reicenberger, H. Jakobs, P. Bastian, R. Helmig, A mixed-dimensional finite volume method for multiphase flow in fractured porous media, Adv. Water Resourc. **29**, pp. 1030–1036, 2006.
[49] S. Rivas-Gomez, J. Cruz-Hernandez, J.A. Gonzalez-Guevara, A. Pineda-Munoz, Block Size and Fracture Permeability in Naturally Fractured Reservoirs, *Abu Dhabi International Petroleum Exhibition and Conference*, 13-16 October 2002.
[50] R.A. Salathiel, Oil Recovery by Surface Film Drainage in Mixed-Wettability Rocks, *Journal of Petroleum Technology*, **25** (10), pp. 1216–1224, 1973.
[51] S.M. Skjaeveland, L.M. Siqveland, A. Kjosavik, W.L.H. Thomas and G.A. Virnovsky, Capillary pressure correlation for mixed-wet reservoirs, *SPE Res Eval & Eng* **3**, 2000.
[52] H. Salimi and J. Bruining, The Influence of Heterogeneity, Wetting, and Viscosity Ratio on Oil Recovery From Vertically Fractured Reservoirs, *SPE J.*, **16** (2), 411–428, 2011.
[53] T.H Sande, I. Berre, J.M. Nordbotten, An efficient multi-point flux approximation method for Discrete FractureMatrix simulations, *J. Comput. Phys.* **231**, 3784–3800, 2012.
[54] K.S Schmid, S. Geiger, and K.S. Sorbie, Semianalytical solutions for cocurrent and countercurrent imbibition and dispersion of solutes in immiscible two-phase flow, *Water Resour. Res.* **47** (2), 2011.
[55] K.S Schmid and S. Geiger, Universal scaling of spontaneous imbibition for water-wet systems, *Water Resour. Res.* **48** (2), 2012.
[56] K.S Schmid and S. Geiger, Universal scaling of spontaneous imbibition for arbitrary petrophysical properties: Water-wet and mixed-wet states and Handy's conjecture, *J. Pet. Sci. Eng.* **101**, 44–61, 2013.
[57] K.S Schmid, S. Geiger, K.S. Sorbie, Higher order FEFV method on unstructured grids for transport and two-phase flow with variable viscosity in heterogeneous porous media, *J. Comput. Phys.* **241**, 416–444, 2013.
[58] J. Tecklenburg, I. Neuweiler, M. Dentz, J. Carrera, S. Geiger, C. Abramowski, O. Silva, A non-local two-phase flow model for immiscible displacement in highly heterogeneous porous media and its parametrization, *Adv. in Water Res.* Available online 5 June 2013, ISSN 0309-1708, http://dx.doi.org/10.1016/j.advwatres.2013.05.012.
[59] I.E. Terez and A. Firoozabadi, Water injection in a water-wet fractured porous media: Experiments and a new model with modified Buckley-Leverett theory, *SPE J.*, **4** (2), 134–141, 1999.
[60] E. Unsal, S.K. Matthäi, and M.J. Blunt, Simulation of multiphase flow in fractured reservoirs using a fracture-only model with transfer functions, *Comput. Geosci.* **14**, pp.527–538, 2010.
[61] P.H. Valvatne, and M.J. Blunt, Predictive pore-scale modeling of two-phase flow in mixed wet media, *Water Resour. Res.* **40** (7), 2004.
[62] M. van Genuchten, A Closed-form Equation for Predicting the Hydraulic Conductivity of Unsaturated Soils, *Soil Sci. Soc. Am. J.* **44**, pp.892–898, 1980.
[63] P. Zhang and T. Austad *Wettability and Oil recovery from Carbonates: Effects of Temperature and Potential Determining Ions*, J. Pet. Sci. Eng., **279**, 179–187, 2006.
[64] X. Zhou, N.R. Morrow and S. Ma, Interrelationship of Wettability, Initial Water Saturation, Aging Time, and Oil Recovery by Spontaneous Imbibition and Waterflooding, SPE J., **5** (2), 199–207, 2000.
[65] Y. Zhou, J.O. Helland and D.G. Hatzignatiou, A Dimensionless Capillary Pressure Function for Imbibition Derived From Pore-Scale Modeling in Mixed-Wet-Rock Images, SPE J., **18** (2), 296–308, 2013.
[66] L. Yu, H. Kleppe, T. Kaarstad, S.M. Skjaeveland, S. Evje, I. Fjelde, Modelling of wettability alteration processes in carbonate oil reservoirs, *Networks and Heterogeneous Media*, **3** (1), pp. 149–183, 2008.